Inhibition of calpain 1 restores plasma membrane stability to pharmacologically rescued Phe508del-CFTR variant

Received for publication, April 4, 2019, and in revised form, July 1, 2019 Published, Papers in Press, July 19, 2019, DOI 10.1074/jbc.RA119.008738

Ana M. Matos[‡§], Francisco R. Pinto[§], Patrícia Barros[‡§], Margarida D. Amaral[§], Rainer Pepperkok[¶], and Paulo Matos[‡§1]

From the [‡]Department of Human Genetics, National Health Institute Doutor Ricardo Jorge, 1649-016 Lisboa, Portugal, the [§]University of Lisboa, Faculty of Sciences, BioISI–Biosystems & Integrative Sciences Institute, 1749-016 Lisboa, Portugal, and the [¶]Cell Biology and Biophysics Unit and Advanced Light Microscopy Facility, European Molecular Biology Laboratory, 69117 Heidelberg, Germany

Edited by Roger J. Colbran

Cystic fibrosis (CF) is a genetic disease caused by mutations in the gene encoding CF transmembrane conductance regulator (CFTR), a chloride channel normally expressed at the surface of epithelial cells. The most frequent mutation, resulting in Phe-508 deletion, causes CFTR misfolding and its premature degradation. Low temperature or pharmacological correctors can partly rescue the Phe508del-CFTR processing defect and enhance trafficking of this channel variant to the plasma membrane (PM). Nevertheless, the rescued channels have an increased endocytosis rate, being quickly removed from the PM by the peripheral protein quality-control pathway. We previously reported that rescued Phe508del-CFTR (rPhe508del) can be retained at the cell surface by stimulating signaling pathways that coax the adaptor molecule ezrin (EZR) to tether rPhe508del-Na^+/H^+-exchange regulatory factor-1 complexes to the actin cytoskeleton, thereby averting the rapid internalization of this channel variant. However, the molecular basis for why rPhe508del fails to recruit active EZR to the PM remains elusive. Here, using a proteomics approach, we characterized and compared the core components of wt-CFTR– or rPhe508del-containing macromolecular complexes at the surface of human bronchial epithelial cells. We identified calpain 1 (CAPN1) as an exclusive rPhe508del interactor that prevents active EZR recruitment, impairs rPhe508del anchoring to actin, and reduces its stability in the PM. We show that either CAPN1 down-regulation or its chemical inhibition dramatically improves the functional rescue of Phe508del-CFTR in airway cells. These observations suggest that CAPN1 constitutes an appealing target for pharmacological intervention, as part of CF combination therapies restoring Phe508del-CFTR function.

The cystic fibrosis (CF)[2] transmembrane conductance regulator (CFTR) is a multispanning cAMP-regulated chloride channel primarily localized to the apical membrane of polarized epithelial cells (1). Mutations in the CFTR gene cause the complex inherited disorder CF (1, 2). The most common CFTR mutation is the deletion of phenylalanine 508 (Phe508del), with ~85% of all CF patients having at least one copy of the Phe508del mutant (Welcome to CFTR2 website, https://www.cftr2.org/)[3] (4). This mutation is mainly characterized by protein misfolding and premature degradation by the endoplasmic reticulum (ER) quality control, preventing the mutant protein from trafficking to the cell surface (5–7). Although Phe508del ER retention is not complete, the very small fraction of channels that reach the cell surface possesses only partial activity because of a gating defect (5, 8, 9) and show a severely decreased plasma membrane (PM) half-life, because of accelerated endocytosis and lysosomal degradation (10, 11).

At present, there are two approved corrector drugs that target the molecular defects in Phe508del (12–14). The first to be used in the clinic is the drug Orkambi®, which combines "corrector" VX-809 (lumacaftor) and "potentiator" VX-770 (ivacaftor). VX-809 is an extensively characterized pharmacological chaperone that promotes folding of Phe508del-CFTR during its biogenesis and processing in the ER (16–19), whereas VX-770 increases CFTR channel open probability (20). Although beneficial, results from clinical trials with this combination therapy have shown only modest efficacy in restoring Phe508del-CFTR function in patients (21–26). Not significantly different are results with the combination drug Symdeko®/Symkevi® (corrector VX-661/teza-

This work was supported by Grants PTDC/BIA-CEL/28408/2017 and IF2012 (to P. M.) and Center Grant UID/MULTI/04046/2019 to BioISI, both from the Fundação para a Ciência e a Tecnologia. This work was also supported by Fellowship SFRH/BD/52490/2014 from BioSYS Ph.D. Program PD65-2012 (to A. M. M.), and Fellowship SFRH/BPD/94322/2013 (to P. B.), both funded by the Fundação para a Ciência e a Tecnologia. The authors declare that they have no conflicts of interest with the contents of this article.
This article contains Tables S1–S9.

[1] To whom correspondence should be addressed: Dept. of Human Genetics, National Health Institute Doutor Ricardo Jorge, Av. Padre Cruz, 1649-016 Lisboa, Portugal. Tel.: 351-217-519-380; E-mail: paulo.matos@insa.min-saude.pt.

[2] The abbreviations used are: CF, cystic fibrosis; CFTR, CF transmembrane conductance regulator; PM, plasma membrane; NHERF1, Na^+/H^+-exchange regulatory factor-1; CAPN1, calpain 1; ER, endoplasmic reticulum; IP, immunoprecipitation; Ab, antibody; PCS, protein confidence score; CCS, combined confidence score; PBMC, peripheral blood mononuclear cell; WB, Western blotting; GLUT-1, glucose transporter 1; HS-YFP, halide-sensitive yellow fluorescent protein; Fsk, forskolin; Gen, genistein; TS, thermal shift; ddH_2O, double-distilled H_2O; DAPI, 4′,6-diamidino-2-phenylindole; PD, pulldown; ANOVA, analysis of variance; ALLM, *N*-acetyl-L-leucyl-L-leucyl-L-methioninal; Dox, doxycycline; EZR, ezrin; CAPNS1, calpain small subunit 1; inh172, CFTR-specific inhibitor 172.

[3] Please note that the JBC is not responsible for the long-term archiving and maintenance of this site or any other third party hosted site.

caftor with potentiator VX-770/ivacaftor) (25–27). Given the complexity of Phe508del-CFTR protein defects (6, 18), part of the incomplete effectiveness of the existing combination therapies is likely to derive from an inability to retain sufficient CFTR levels at the apical surface of epithelial cells. Indeed, we and others have shown that the PM stability of chemical chaperone-rPhe508del-CFTR is still dramatically inferior to that of WT (wt)-CFTR, because of its targeting by the peripheral protein quality control and its deficient anchoring to the actin cytoskeleton (10, 28, 29). Notwithstanding, and despite the potential for greater clinical effectiveness of newer investigational corrector combinations (30, 31), there are no therapeutic strategies specifically designed to target the decreased PM stability of chemically rPhe508del-CFTR.

Previously, we demonstrated that the anchoring of rescued channels to the actin cytoskeleton can be enhanced by promoting the PDZ-mediated interaction of Phe508del-CFTR with the Na^+/H^+ exchange regulatory factor-1 (NHERF1) and the actin-binding adaptor protein ezrin (EZR) (28, 29). We have also shown that the mechanism behind this PM stabilization lies on a conformational change in NHERF1, triggered by EZR activation through RAC1 signaling, which is then able to bind and stabilize misfolded CFTR at the PM (29). This strongly indicated that the protein interactions of wt- and rPhe508del-CFTR at the cell surface can constitute major determinants of CFTR stability and retention at the PM.

Over the last years, a growing number of proteins have been reported to interact with PM CFTR, possibly participating in the assembly of large macromolecular complexes (32, 33). Most interactions occur through the N terminus, the regulatory domain, or the C-terminal tail of CFTR, either directly or mediated through various PDZ domain-containing proteins (32, 34, 35). These dynamic interactions impact on channel function, as well as on its processing and localization within cells (32, 33). Furthermore, it has been established that mutant and nonmutant CFTR show considerable differences in their whole cell interactomes, and thus these differential protein interactions may contribute to the defects observed in Phe508del-CFTR processing and function (36). Hence, although several CFTR interactor partners are known (33, 36, 37), there is no study describing specifically CFTR's particular interactome at the PM, whether differences between wt- and pharmacologically rescued Phe508del-CFTR occur (38), and how these differences could contribute to the defective function and stability of the rescued mutant channels.

Here we propose to address these questions by identifying the core components of the CFTR PM molecular complexes in human airway cells expressing wt- or Phe508del-CFTR. For this, we developed an immunoprecipitation (IP) method that selectively captures the CFTR-containing macromolecular complexes at the PM. Our data reveal significant differences between the PM interactors of wt and rPhe508del-CFTR and allowed us to identify calpain 1 (CAPN1) protease as a key player in reducing Phe508del-CFTR actin anchoring and PM stability, thus contributing to the decreased cell surface retention of this rescued mutated channel.

Results

wt-CFTR and corrected rPhe508del-CFTR assemble different PM protein interactors

We first determined whether wt-CFTR and rPhe508del-CFTR have different PM protein interactors that could contribute to their distinct cell surface stabilities. For that, we developed an IP protocol that allows to biochemically capture PM CFTR-selective interactomes. Briefly, using a cell line model (mCherry–FLAG–CFTR CFBE cells (39)) that stably expresses mCherry-fused CFTR protein with a FLAG epitope tag inserted at the fourth extracellular loop, we were able to exclusively label CFTR proteins at the PM by incubating cells at 4 °C with an anti-FLAG antibody (Ab) without permeabilization. We then used dithiobis (succinimidyl propionate) (short spacer) and Succinimidyl 3-(2-pyridyldithio)propionate (long spacer) cross-linkers to reversibly bind, at 4 °C, both the Ab (extracellularly) and the intracellular proteins associated with CFTR at the PM (Fig. 1, *A* and *B*). The same protocol was applied in parallel to CFBE cells expressing either wt- or Phe508del–mCherry–FLAG–CFTR, the latter rescued either by low temperature (26 °C) or by VX-809 treatment (Fig. 1*C* and "Experimental procedures").

As part of the optimization process, we scaled up the number of cells in the Phe508del-CFTR experiments, so that the total amount of rescued CFTR (band C) in the IP was roughly equivalent to that of wt-CFTR (Fig. 1*D*). To control the experiment for background IP contaminants we used, for wt-CFTR, cell extracts incubated with G-protein agarose beads but without the anti-FLAG Ab. For Phe508del-CFTR IPs, lysates from cells incubated at 37 °C (that have none to residual levels of band C at the PM) were considered the most reliable control for proteins co-IPed with rPhe508del-CFTR (Fig. 1*C*). The recovered proteins were first analyzed by SDS-PAGE followed by MS-compatible silver staining (40) (Fig. 2).

Noticeably, a distinct band profile was observed for each condition, suggestive of different co-precipitate compositions (Fig. 2). These profiles were reproducible between experimental replicates, and therefore, the whole samples of three individual assays were sent to MS analysis.

Bioinformatic analysis of MS data highlighted a candidate interactor potentially involved in the PM destabilization of rPhe508del-CFTR

Qualitative nano-LC MS/MS analysis of our samples generated a set of data in which each MS spectra protein hit was characterized by a protein confidence score (PCS) given by the SCIEX proprietary ProteinPilot™ software. For PCS $>$ 1.3, the confidence in the identification of that particular peptide is equal or higher than 95%. Given that all the experiments were performed in triplicate, we created an algorithm to generate a combined confidence score (CCS), producing five additional integrated confidence levels for the proteins detected among the different replicates: level 5 proteins are detected with PCS $\geq$ 1.3 in more than one replicate and not in the controls; level 4 proteins are detected in one replicate with a PCS $\geq$ 1.3 and not in the controls; level 3 proteins are detected in more replicates than in controls with an average PCS higher than their respec-

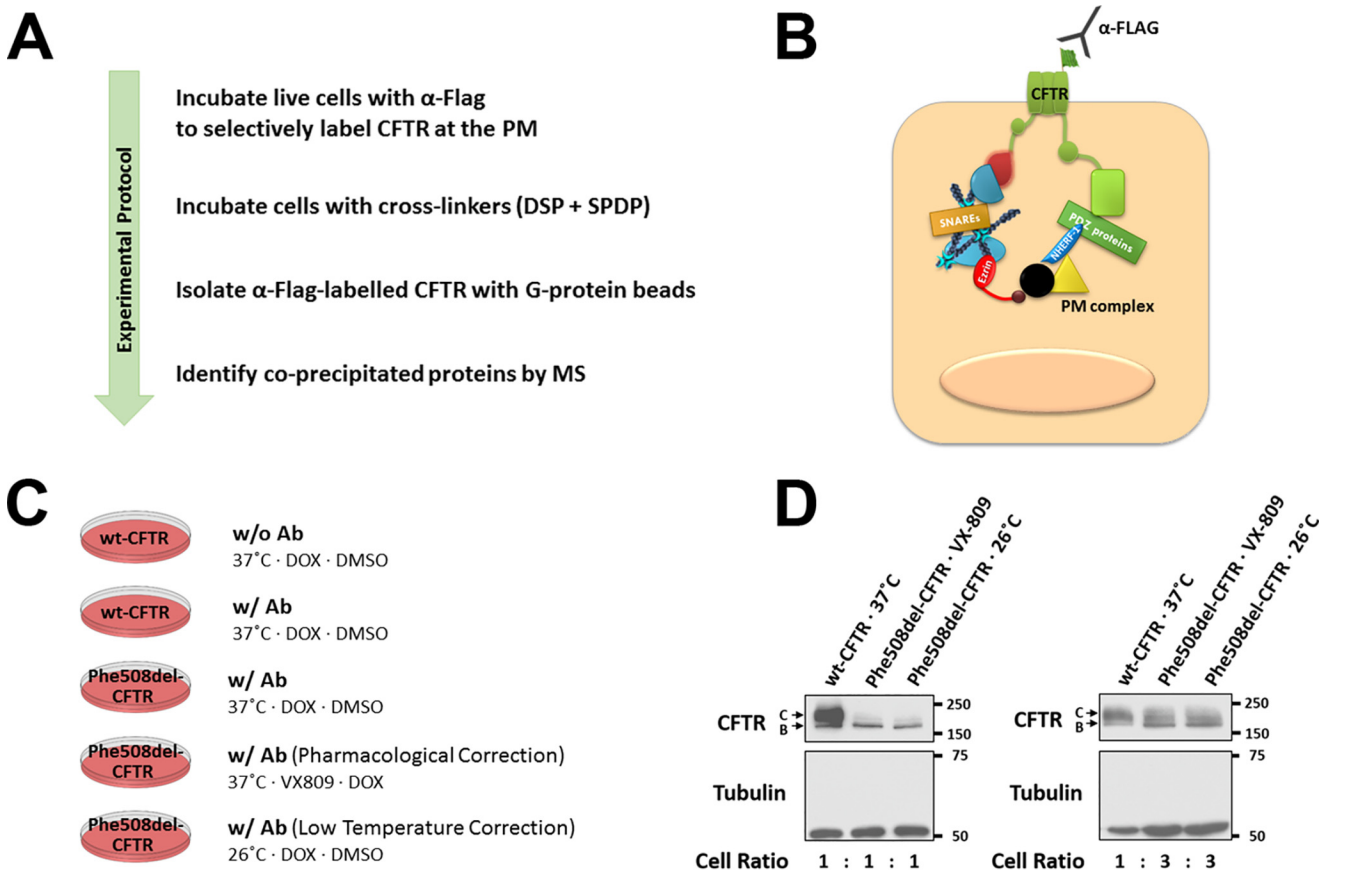

Figure 1. Selective IP of CFTR membrane association complexes. *A*, summary of the protocol used for the precipitation of CFTR membrane association complex. CFTR-containing complexes at the PM were selectively immunolabeled on ice using an Ab specifically recognizing the extracellular FLAG tag. Following cross-link and lysis, these complexes were immunoprecipitated, resolved in an SDS-PAGE gel, silver-stained, and then sent to MS analysis. *B*, schematic representation of putative CFTR-containing macromolecular complex at the PM, after immunolabeling and cross-linking. *C*, diagram of the experimental conditions used. mCherry–FLAG–wt-CFTR CFBE cells were incubated at 37 °C, whereas mCherry–FLAG–Phe508del-CFTR cells were incubated in three different conditions: at 37 °C; at 26 °C (for low temperature Phe508del rescue); and with VX-809 (for Phe508del pharmacological correction). An additional control set of wt-CFTR cells, incubated at 37 °C, were prepared with no FLAG antibody added. CFTR expression in all cells was induced by incubation with 1 μg/ml Dox for 48 h. *D*, illustrative WB of wt-CFTR cells and Phe508del-CFTR, cultured in the same conditions, except for the cell quantity, which was modified by using three times more Phe508del-CFTR cells on the *two right panels*. *Arrows* indicate immature (*band B*) and fully glycosylated (*band C*) CFTR. Equivalent conditions were used in the three independent experiments sent to MS analysis.

tive controls; level 2 proteins are detected in one replicate with a PCS $\leq$ 1.3 and not in the controls; and level 1 are proteins detected in the same number of replicates and controls, with an average replicate PCS higher than the average PCS in the corresponding controls.

Altogether, we detected 481 wt-CFTR PM putative protein interactors and 631 and 660 Phe508del-CFTR PM putative interactors, respectively, rescued by pharmacological and low temperature, most of which have low CCS scores (Fig. 2*B* and Tables S1–S3). Given that cross-linking agents were used, it is highly likely that many of these proteins could be indirect or nonspecific interactors present in other PM complexes that share or interact with proteins present in CFTR-containing PM complexes. Notably, most proteins from both Phe508del rescued conditions overlap, sharing 533 protein putative interactors (Fig. 2*B*). Interestingly, ~40% (337 of 855) of all identified proteins are common between all data sets (Fig. 2*C* and Table S4), possibly containing the proteins that form the core PM CFTR interactome. For downstream analyses, only high confidence level proteins (>95% confidence, *i.e.* CCS of 4 or 5) were considered. This approach restricted the list of putative CFTR interactors to 56 high confidence proteins in wt-CFTR, whereas the number of high confidence proteins in complex with rPhe508del-CFTR was considerably larger, comprising 225 in pharmacological rescued and 245 in low-temperature rPhe508del-CFTR, of which 158 were common to both data sets (Fig. 2*D* and Table S5). By crossing our results with the whole cells CFTR interactome obtained by Pankow *et al.* (36), we observed that 23 of the 56 (~41%) proteins detected with high confidence in wt-CFTR complexes at the PM and 49 of the 158 (~30%) co-detected with PM–rPhe508del-CFTR were identified by both studies (Fig. 2*E* and Tables S6 and S7).

Because both low temperature and VX-809 treatment produce rPhe508del-CFTR proteins with equally decreased PM half-lives (41), we postulated that it would be highly likely that any interactors influencing rPhe508del-CFTR surface stability should be among the proteins shared by PM complexes produced by either rescue approach. Our previous data (29) also indicated that these unknown destabilizing factors should be proteins interacting differentially with wt- and rPhe508del-CFTR at the PM. Therefore, we narrowed the list of proteins

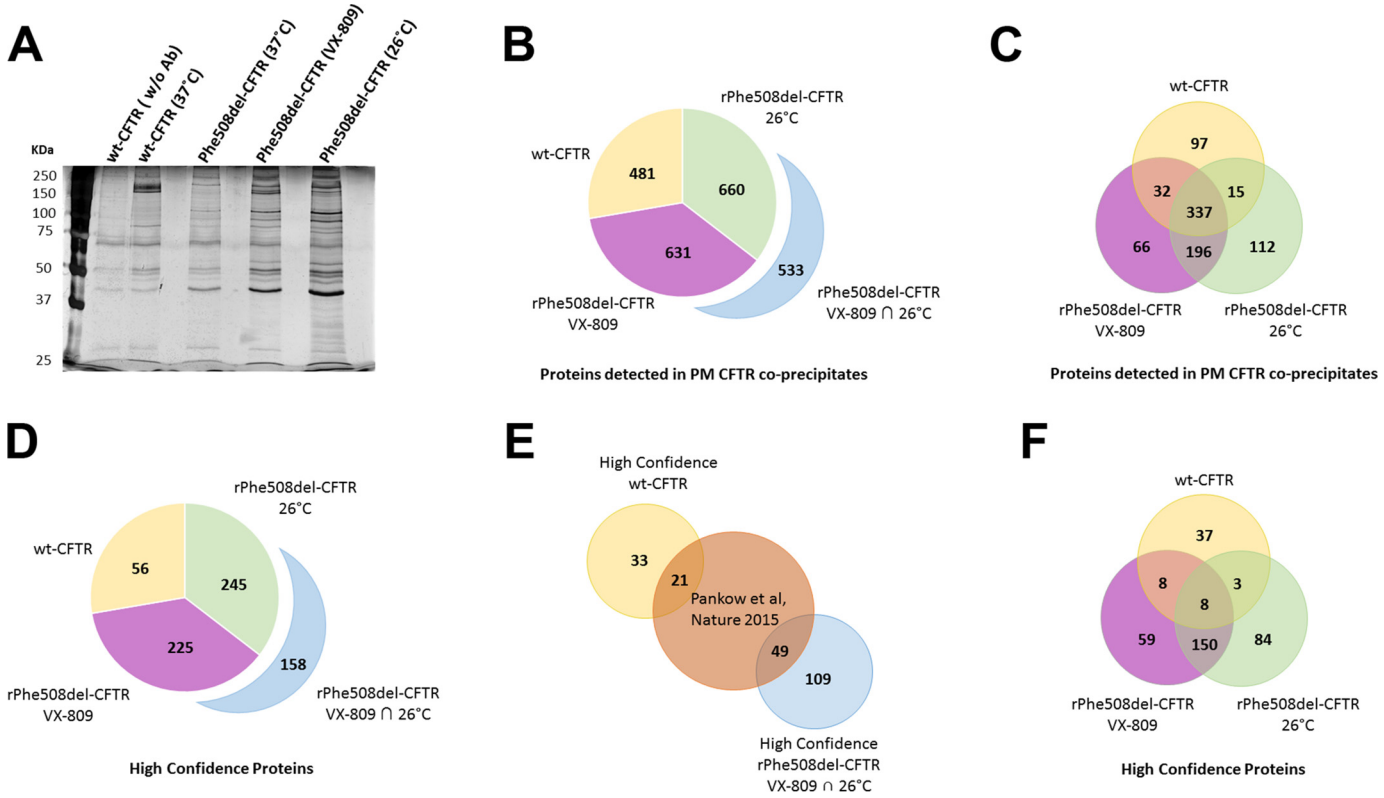

Figure 2. Proteins detected in the different putative interactomes of wt- and rPhe508del-CFTR at the PM. *A*, representative gel showing the band profile of the PM CFTR co-precipitates observed in the three independent IP experiments sent for MS analysis. PM CFTR co-immunoprecipitates from each experimental condition were de–cross-linked with 100 mM DTT, separated on a 9% (w/v) SDS-PAGE gel, and silver-stained. Note that although there are a few common bands, particular band patterns are observable for each experimental condition. *B*, graph representing the number of CFTR interactors detected by qualitative nano-LC MS/MS analysis in wt-CFTR (*yellow*) and Phe508del-CFTR, rescued either by pharmacological rescue with VX-809 (*purple*), or by low temperature at 26 °C (*green*). In *blue* is the number of proteins in common between the rescued conditions. *C*, Venn diagram of CFTR interactors represented in *B*. *D*, graph representing the number of CFTR interactors detected with a high confidence score (CCS of 4 or 5) in wt-CFTR and Phe508del-CFTR, rescued either by pharmacological rescue with VX-809 or by low temperature at 26 °C, and their common proteins. *E*, Venn diagram with the intersection of the whole CFTR interactome detected as described in Ref. 36 and our high confidence PM CFTR interactors in wt-CFTR and rPhe508del-CFTR. *F*, Venn diagram of CFTR interactors represented in *D*.

putatively influencing rPhe508del-CFTR PM stability by intersecting the groups of high-confidence proteins in the low temperature and VX-809 –treatment data sets and excluding those that also co-precipitated with wt-CFTR. With this approach, we further restricted our candidate list to 150 proteins (Fig. 2*F* and Table S5). Next, we investigated which proteins in this narrowed list were reportedly functionally related. For that, we extracted known physical protein interactions from curated human interactome databases (see "Experimental procedures") to build an integrated network of candidate protein interactions. We found that, from the 150 putative interactors interfering with rPhe508del-CFTR stability, 135 (90%) formed a tightly connected network around CFTR, with 539 interactions (Fig. S1 and Table S8). This means that available interactome data supports the close relationship between most of the proteins here detected as specifically interacting with rPhe508del-CFTR at the PM, both upon VX-809 and low-temperature treatment. This is not unexpected because most of the recorded interactions in public databases result from whole cell studies, and many of these proteins may, at one point, interact with CFTR or with proteins that interact directly or indirectly with CFTR.

Having previously shown that rPhe508del-CFTR destabilization at the cell surface results from an interference with the formation of the CFTR–NHERF1–EZR retention complex at the PM (28, 29, 42), we further restricted this network to proteins annotated as direct interactors of either EZR, NHERF1, or CFTR. This approach generated a subnetwork of 22 proteins (Fig. 3 and Table S9) that we selected as the core of putative candidates involved in destabilizing rPhe508del-CFTR-containing complexes at the PM.

Gene ontology-based functional annotation analysis of these 22 hit proteins using DAVID (Database for Annotation, Visualization and Integrated Discovery, https://david.ncifcrf.gov/) (3, 15)[3] revealed that, as expected, all 22 proteins are known to participate in macromolecular protein complexes. Interestingly, 52% of these proteins are annotated as being localized at the membrane, and 64% are annotated as being localized at the cytosol (Table S10). Both subcellular localizations are expected for such a large and dynamic protein complex, because both the N and C termini of CFTR are in the cytoplasm and mediate its interaction with large clusters of PDZ adaptor and functionally related proteins (32, 33).

To infer the potential relevance of each of these 22 proteins to the assembly of rPhe508del-CFTR–NHERF1–EZR complexes at the PM, we devised a scoring formula that measures the contribution of each node to the establishment of molecular bridges between these three proteins. Bridges involving more

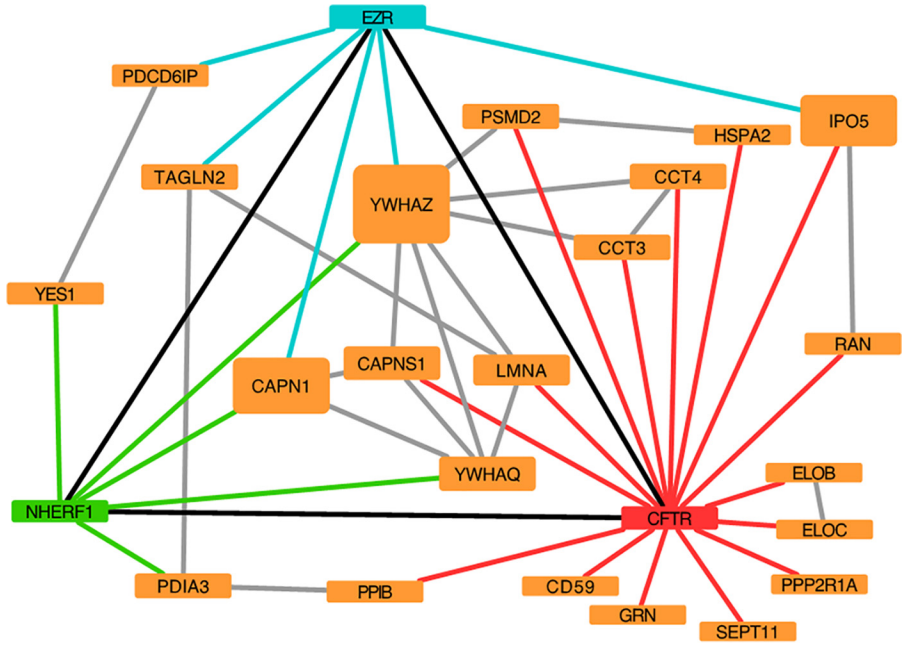

Figure 3. Subnetwork of 22 proteins with direct interactions to CFTR, EZR, or NHERF1. Schematic representation of the 22 proteins network with direct interactions to CFTR, EZR, or NHERF1 that were detected with high confidence interacting with rPhe508del-CFTR at the PM, through the action of both VX-809 and low temperature. The sizes of the *orange node boxes* represent a visual score of putative relevance of the protein to the formation of the CFTR–EZR–NHERF1 complex.

proteins were given a lower weight in the final score (see "Experimental procedures").

This analysis, depicted in Fig. 3 by the size of node boxes, identified proteins YWHAZ (14-3-3ζ), CAPN1 (calcium-activated neutral proteinase 1, catalytic subunit, also calpain 1), and IPO5 (importin 5) as the most relevant in this context. IPO5 is a direct interactor of CFTR and EZR, whereas YWHAZ and CAPN1 interact directly with EZR and NHERF1. YWHAZ reaches a higher score because it interacts directly with five CFTR direct neighbors. CAPN1 can also form a complex with its small regulatory subunit–calpain small subunit 1 (CAPNS1). Remarkably, the CAPN1–CAPNS1 complex interacts directly with CFTR, EZR, and NHERF1 (Fig. 3).

The proteins in this list were also intersected with the druggable proteome at the ChEMBL database to identify the most likely druggable hits. This intersection highlighted CAPN1 as a particularly strong candidate.

CAPN1 is a strong candidate for selective interaction with rPhe508del-CFTR

CAPN1 belongs to a group of calcium-sensitive cysteine proteases that are ubiquitously expressed in human cells and associated with subcellular organelles such as the cytoskeletal actin filaments, vesicles, and the PM (43). Furthermore, CAPN1 inhibition was shown to promote the partial rescue of Phe508del-CFTR in peripheral blood mononuclear cells (PBMCs) from CF patients (44).

To assess the robustness/directness of the interaction between PM-CFTR and CAPN1, we performed the same IP protocol, but in the absence of cross-linking agents. We confirmed that CAPN1 co-precipitates with rPhe508del-CFTR but not with wt-CFTR, even in the absence of cross-linking agents, showing the strength of this interaction (Fig. 4). In contrast,

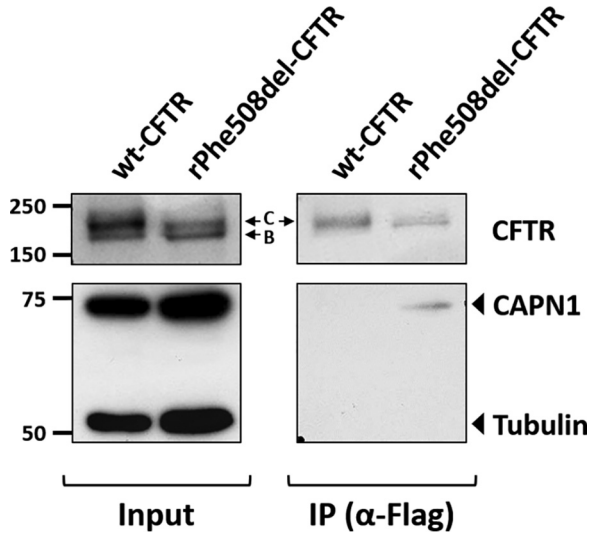

Figure 4. Validation of CAPN1 as a hit protein that specifically associates with rPhe508del-CFTR at the PM. WB analysis of proteins in the co-IP with FLAG-tagged wt- or rPhe508del-CFTR at the cell surface, with the latter rescued to the PM by 48 h of incubation with 3 μM VX-809. Shown are representative images of three independent validation experiments.

tubulin, which was consistently absent from the isolated CFTR-containing PM-associated complexes, was also absent from the un–cross-linked co-precipitates, confirming the specificity of CAPN1 detection in the co-IP (Fig. 4). We therefore decided to study the effect of CAPN1 on the PM stability of rPhe508del-CFTR.

CAPN1 down-regulation increases the PM abundance and function of VX-809–rPhe508del-CFTR

Using a CAPN1-specific siRNA, we down-regulated CAPN1 expression in CFBE cells to ~32% of its normal levels (Fig. 5*A*)

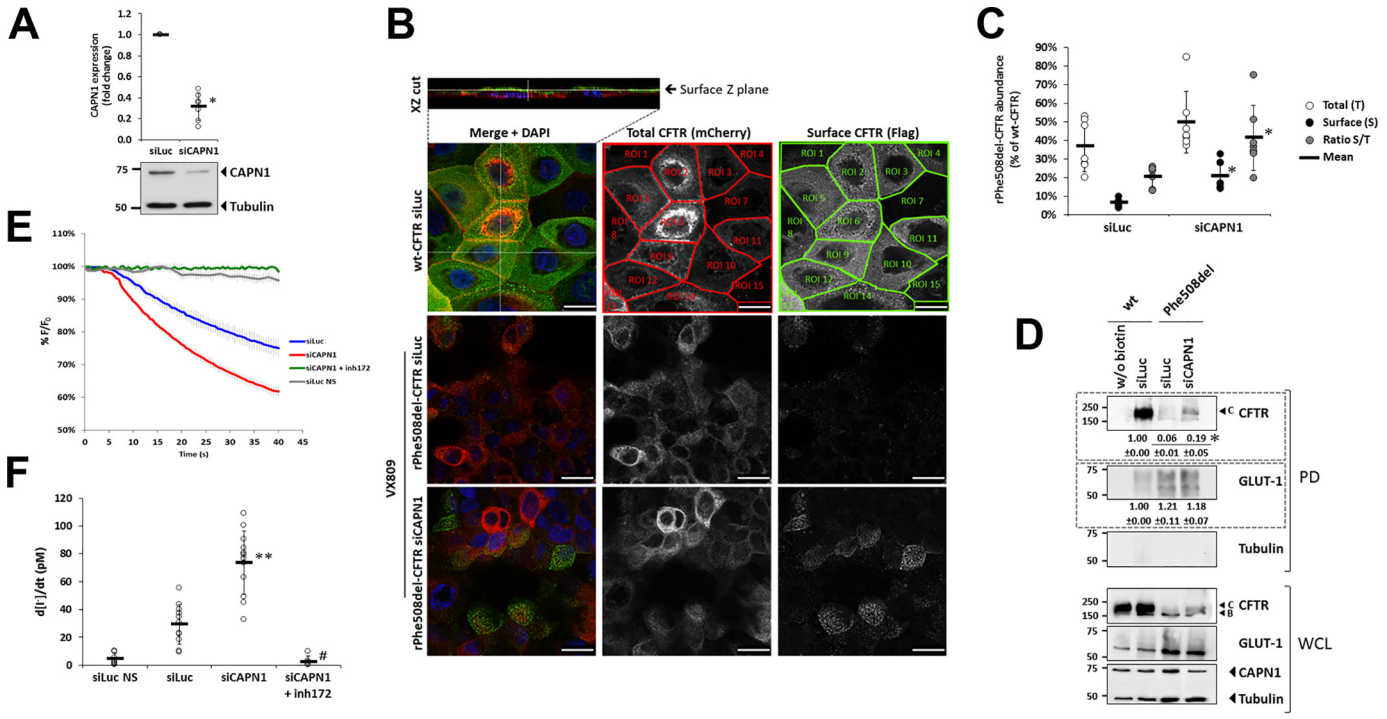

Figure 5. CAPN1 down-regulation increases the levels and function of PM rPhe508del-CFTR. *A*, assessment of CAPN1 siRNA-mediated knockdown efficiency. The data are shown as fold change relative to siLuc (control). *B*, confocal images of Dox-induced mCherry–FLAG–wt-CFTR or Phe508del-CFTR cells, transfected with either siLuc or siCAPN1. Phe508del-CFTR was rescued to the PM by 48 h of incubation with 3 μM VX-809 at 37 °C. Images are triple-labeled nonpermeabilized cells, in which mCherry fluorescence is proportional to the total amount of CFTR, Alexa Fluor 488 fluorescence is proportional to the amount of CFTR present at the cell surface, and nuclei are stained with DAPI. A 0.2-μm *Z*-stack of 1 Airy confocal images were acquired (*top left insert*) to select the best XY plane to analyze the CFTR protein at the cell surface. ImageJ software (National Institutes of Health) was used to delimitate each single cell as individual regions of interest so as to allow measurement of mCherry (*red-lined lattice*) and Alexa Fluor 488 (*green-lined lattice*) fluorescence signal intensities. Note that high intensity, perinuclear mCherry signals indicate cells that are cross-sectioned at the considered XY confocal plane (*e.g.* regions of interest 2 and 6 in the *top panels*). Because they are not surface-representative signals, these areas were excluded from the quantitative analysis. *Scale bars* correspond to 25 μm. *C*, analysis of single-cell fluorescence signals in three independent experiments. The data are presented as total (*T*), surface (*S*), or *S*/*T* ratio of rPhe508del-CFTR abundance, expressed as percentages of wt-CFTR values. *D*, WB analysis of biotinylated cell surface proteins (biotin PD) and whole-cell lysates (*WCL*) treated as in *B*. *E*, traces of iodide-induced HS-YFP fluorescence decay of Phe508del-CFTR CFBE cells treated with 3 μM VX-809 for 48 h, transfected with either siLuc or siCAPN1, and co-treated, or not, with 25 μM of inh172 for 15 min prior to stimulation (or not; *NS* indicates no stimulation) for 30 min in PBS with Fsk and Gen, in the presence or absence of inh172, followed by continuous fluorescence recording and addition of I^- (100 mM). *F*, summary of iodide influx rates calculated by fitting the iodide assay results to exponential decay curves. One-way ANOVA analysis detected significant differences between treatments ($F = 44.862$; $p < 0.001$). Post hoc Tukey's tests were used to identify significant variations relative to siLuc (**, $p < 0.001$) or siCAPN1 (#, $p < 0.001$) alone. The figure shows representative images and quantification results of seven independent experiments. The means ± S.D. are given for all quantified data, highlighted by *dotted gray rectangles* in *D*. For *A*, *C*, and *D*, significance was tested using unpaired, two-tailed *t* tests, comparing siCAPN1 to siLuc (*, $p < 0.01$).

and then assessed the PM abundance of VX-809 –rPhe508del-CFTR under these conditions. For this, we performed a cell surface protein immunolabeling assay that allows the selective labeling of CFTR proteins at the PM (Ref. 39; see also "Experimental procedures"). Briefly, Phe508del-CFTR PM expression was rescued by VX-809 treatment (48 h at 37 °C) in mCherry–FLAG–Phe508del-CFTR CFBE cells transfected with either siCAPN1 or siLuc (used as control). The cells were then placed at 4 °C to arrest endocytic traffic, and without permeabilization, Phe508del-CFTR protein at the cell surface was labeled with anti-FLAG Ab, followed by detection with an Alexa Fluor 488 –conjugated secondary Ab. Confocal images selectively capturing the cell surface plane clearly show that CAPN1 down-regulation increased PM expression of rPhe508del-CFTR, when compared with siLuc control (Fig. 5*B*). Quantification of membrane (Alexa Fluor 488) CFTR signals (Fig. 5*C*) revealed that this increase is statistically significant, corresponding to a 3-fold increment in the PM abundance of VX-809 –rPhe508del-CFTR (from 7 to 21% of wt-CFTR signal). Quantification of total CFTR (signal from CFTR N-terminal mCherry tag) showed that CAPN1 down-regulation also slightly increased the overall abundance of Phe508del-CFTR in these cells, albeit not significantly. Accordingly, the ratio of cell surface/total CFTR signals evidenced a significant >2-fold increase in CFTR abundance at the PM in CAPN1-depleted cells (Fig. 5*C*). These results were further confirmed using a cell surface protein biotinylation assay, where proteins at the cell surface are labeled with nonpermeable EZ-Link Sulfo–NHS-SS–Biotin and captured with streptavidin–agarose beads (Fig. 5*D*). Western blotting (WB) analysis of biotin precipitates from CFBE cells, treated as before, confirmed an increase in rPhe508del-CFTR abundance at the cell surface upon CAPN1 down-regulation, compared with control cells (siLuc). Moreover, detection of glucose transporter 1 (GLUT-1), an integral membrane protein transporter of glucose of mammalian cells, in these samples showed no noticeable variation in the abundance of this transporter at the cell surface, indicating the specificity of the CAPN1 down-regulation effect on increasing rPhe508del-CFTR PM levels (Fig. 5*D*). Next, we evaluated how CAPN1 down-regulation impacted the functional rescue of Phe508del-CFTR by the VX-809 corrector. For this we used the previously described iodide influx assay, based in the halide-sensitive yel-

low fluorescent protein (HS-YFP) (45–47). Briefly, CFBE cells co-expressing Phe508del-CFTR and the HS-YFP mutant (45) were transfected with either siCAPN1 or siLuc and incubated with VX-809 for 48 h (Fig. 5, *E* and *F*).

The cells were then stimulated for 30 min in PBS with 5 μM forskolin (Fsk) and 20 μM genistein (Gen) to induce CFTR activity. Next, a HS-YFP fluorescence baseline was recorded for 5 s, and its decay followed continuously (at 0.5-s intervals) after the rapid (<1 s) addition of iodide (Fig. 5*E*). The curves were fitted to an exponential decay function to derive the initial rates of iodide influx that, as previously described (29), are directly proportional to the extent of chloride effluxed from these cells via CFTR. Consistent with the observed >2-fold increase in PM abundance of VX-809–rPhe508del-CFTR, CAPN1 down-regulation increased by ~2.5-fold the iodide influx rate in these cells, which was specifically dependent on CFTR activity, because the effect was abolished upon treatment with the CFTR-specific inhibitor 172 (inh172) (Fig. 5*F*). Altogether, these results strongly suggest that CAPN1 plays an important role in regulating the overall PM stability of pharmacologically rPhe508del-CFTR at the PM of bronchial epithelial cells.

Knockdown of CAPN1 improves the PM stability of rPhe508del-CFTR through enhanced EZR binding

To determine whether the effect of CAPN1 down-regulation on the increased levels of rPhe508del-CFTR at the cell surface resulted from enhanced stability, we coupled the surface CFTR immunolabeling assay to a previously described surface thermal destabilization assay (29; see Experimental procedures). Briefly, VX-809–rPhe508del-CFTR (48 h) was stabilized at the surface by incubation of the cells at 30 °C. The cells were then shifted for 4 h to 37 °C (thermal shift (TS)), which destabilizes rPhe508del-CFTR at the cell surface causing its internalization, unless additional experimental conditions lead to the retention of the rescued channel at the PM (41, 48). CFTR at the cell surface was immunolabeled and analyzed as before (Fig. 6*A*). Fluorescence signal quantification revealed that upon TS to 37 °C, rPhe508del-CFTR in siLuc-transfected cells was destabilized and removed from the PM, reducing the protein cell surface abundance by ~60% (Fig. 6*B*). In contrast, down-regulation of CAPN1 clearly increased the surface stability of the rescued channels because ~80% of the protein remained at the PM after 4 h at 37 °C (Fig. 6*B*). The immunolabeling results were again confirmed by cell surface protein biotinylation (Fig. 6*C*), which also showed that GLUT-1 PM abundance was not influenced by CAPN1 knockdown, again supporting a CFTR-specific PM retention effect (Fig. 6*C*).

We have previously shown that the critical step to stabilize Phe508del-CFTR at the PM is the opening of NHERF1 PDZ2 domain by the binding of activated EZR (29). Because interaction with CAPN1 was shown to cause the inactivation of EZR (43, 49, 50), we hypothesized that the increased rPhe508del-CFTR PM stability by down-regulating CAPN1 could result from enhancement of its cytoskeletal anchoring by the promotion of rPhe508del-CFTR–NHERF1–EZR interaction. To test this hypothesis, we immunoprecipitated PM–rPhe508del-CFTR in the TS assay conditions used above and analyzed the levels of EZR and NHERF1 in the co-IP (Fig. 6*D*). Notably, whereas the levels of NHERF1 in the co-IP were equivalent between control (siLuc) and siCAPN1 transfected cells, the amount of EZR co-precipitating with PM–rPhe508del-CFTR upon CAPN1 down-regulation increased to levels near those found in wt-CFTR– expressing cells (Fig. 6*D*). These results are in accordance with our hypothesis and show that CAPN1 binding negatively influences the formation of Phe508del-CFTR–NHERF1–EZR anchoring complex, leading to a diminished stability of the pharmacological corrected channels.

Acute chemical inhibition of endogenous calpain 1 significantly increases VX-809–mediated Phe508del-CFTR functional rescue in bronchial epithelial cells

CAPN1 was identified above as a druggable candidate protein because its activity can be chemically inhibited by ALLM, a cell-permeable peptide aldehyde (51, 52). We thus tested the effect of ALLM treatment on the functional rescue of Phe508del-CFTR by VX-809 using the HS-YFP assay. CFBE Phe508del-CFTR cells co-expressing HS-YFP were incubated with 3 μM VX-809 for 48 h and co-treated with either DMSO or 250 nM of ALLM for the last 4 h. As before, the cells were then stimulated with Fsk and Gen and analyzed by live confocal imaging after I^- addition (Fig. 7, *A* and *B*). Treatment with ALLM produced a striking response in fluorescence decay, which was CFTR-dependent, because it was completely inhibited by inh172 (Fig. 7*A*). Calculation of initial iodide influx rates (as before) revealed that treatment with ALLM increased by ~4-fold the functional response of VX-809–rPhe508del-CFTR, when compared with VX-809 + DMSO-treated cells (Fig. 7*B*).

Analysis of PM abundance (Fig. 7*C* and Fig. S2*A*) and surface TS (Fig. 7*E* and Fig. S2B) of rPhe508del-CFTR corroborate this enhanced functional response. ALLM-treated cells presented a 5-fold increase in VX-809–rPhe508del-CFTR PM levels (~8 to ~40%, compared with VX-809 + DMSO control cells; Fig. 7*C*).

Even considering the small enrichment in total CFTR induced by ALLM treatment, the Phe508del-CFTR retention at the PM (surface/total ratio) reached nearly 4-fold that of control, DMSO-treated cells (Fig. 7*C*), which translated into a full thermal stabilization of the rescued channels present at the surface of these cells (Fig. 7*E*). Again, these results were also observable through cell surface protein biotinylation followed by WB analysis (Fig. 7, *D* and *F*, respectively).

Discussion

So far, several studies have identified numerous CFTR interactor proteins with essential roles in the processing, localization, and function of the channel (32–36, 53, 54). Nonetheless, the present work is the first to globally characterize CFTR interactors specifically occurring at the PM. Previous studies have shown that several interactions between CFTR and its binding partners are mediated through the scaffolding protein NHERF1, which seems to be a central protein in the assembly of the CFTR-containing macromolecular complexes at the surface of airway cells (33, 55, 56). EZR is also a key component of these complexes, mediating the tethering of NHERF1-bound CFTR proteins at the PM to the actin cytoskeleton, thus stabilizing the channel at the cell surface by blocking its endocytosis (57–59). Moreover, we also showed previously that the low cell

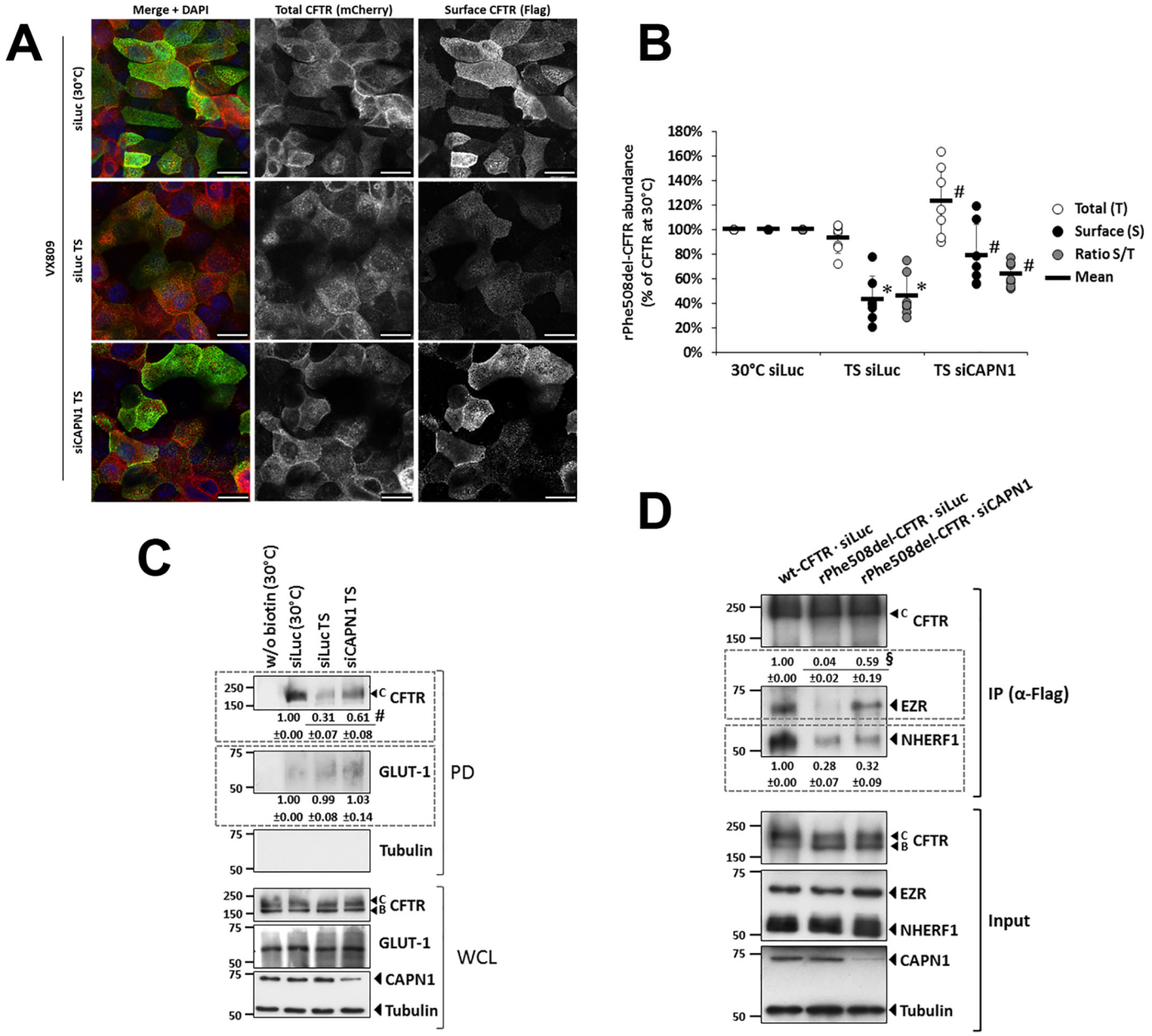

Figure 6. Effect of CAPN1 down-regulation on the levels and thermal stability of PM-associated complexes containing EZR, NHERF1, and rPhe508del-CFTR. *A*, confocal images of Dox-induced CFBE mCherry–FLAG–Phe508del-CFTR cells, transfected with either siLuc or siCAPN1. Phe508del-CFTR was rescued to the PM by 48 h of incubation with VX-809 at 30 °C and subjected to a TS of 4 h at 37 °C, except for siLuc low temperature control (30 °C). Images are triple-labeled unpermeabilized cells, in which mCherry fluorescence is proportional to the total amount of CFTR, Alexa Fluor 488 fluorescence is proportional to the amount of CFTR present at the cell surface, and nuclei are stained with DAPI. *Scale bars* correspond to 25 μm. *B*, analysis of single-cell fluorescence signals in five independent experiments. The data are presented as means ± S.D. of total (*T*), surface (*S*), or *S*/*T* ratio of rPhe508del-CFTR abundance, expressed as percentages of CFTR at 30 °C (low temperature control). *C*, WB analysis of biotinylated cell surface proteins (biotin PD) and whole-cell lysates (*WCL*), treated as in *A*. *D*, WB analysis of EZR and NHERF1 levels co-precipitating with wt- or Phe508del-CFTR at the PM. Phe508del-CFTR cells were treated for 48 h with VX-809 at 30 °C and transfected with either siLuc or siCAPN1. The cells were then subjected to TS for 4 h at 37 °C to destabilize rescued CFTR at the PM. The wt-CFTR cells were maintained always at 37 °C. Surface CFTR was then labeled with anti-FLAG antibody in nonpermeabilizing conditions and immunoprecipitated. WB using specific antibodies detected co-precipitating NHERF1 and EZR proteins. The data in *C* and *D* are representative of three independent experiments, and the *dotted gray rectangles* highlight the respective quantification (means ± S.D.) of CFTR and GLUT-1 abundance at the PM (*C*), relative to siLuc at 30 °C, and of co-precipitating EZR and NHERF1 (*D*), relative to wt-CFTR siLuc. The data significance was tested using unpaired, two-tailed *t* tests, comparing TS siLuc to 30 °C siLuc (*B*; *, $p < 0.001$) and TS siCAPN1 to TS siLuc (*B–D*; #, $p < 0.05$; §, $p < 0.01$).

surface stability of chemically rescued Phe508del-CFTR was, at least in part, caused by an impaired recruitment of EZR to rPhe508del-CFTR–NHERF1 complexes at the PM, preventing their anchoring to actin and thus leading to their rapid internalization (28). Moreover, we and others showed that overexpression of constitutively active EZR coaxed the retention of rPhe508del-CFTR at the PM (29, 60), by causing a conformational change in NHERF1 that displaced CHIP E3-ubiquitin ligase, and thus prevented CFTR ubiquitination and internalization (29). This led us to hypothesize that EZR overexpression was somehow circumventing a mechanistic restrain that prevented its association with rPhe508del-CFTR–NHERF1 complexes in normal conditions. We therefore reasoned that it would be highly likely that, similarly to CHIP, additional pro-

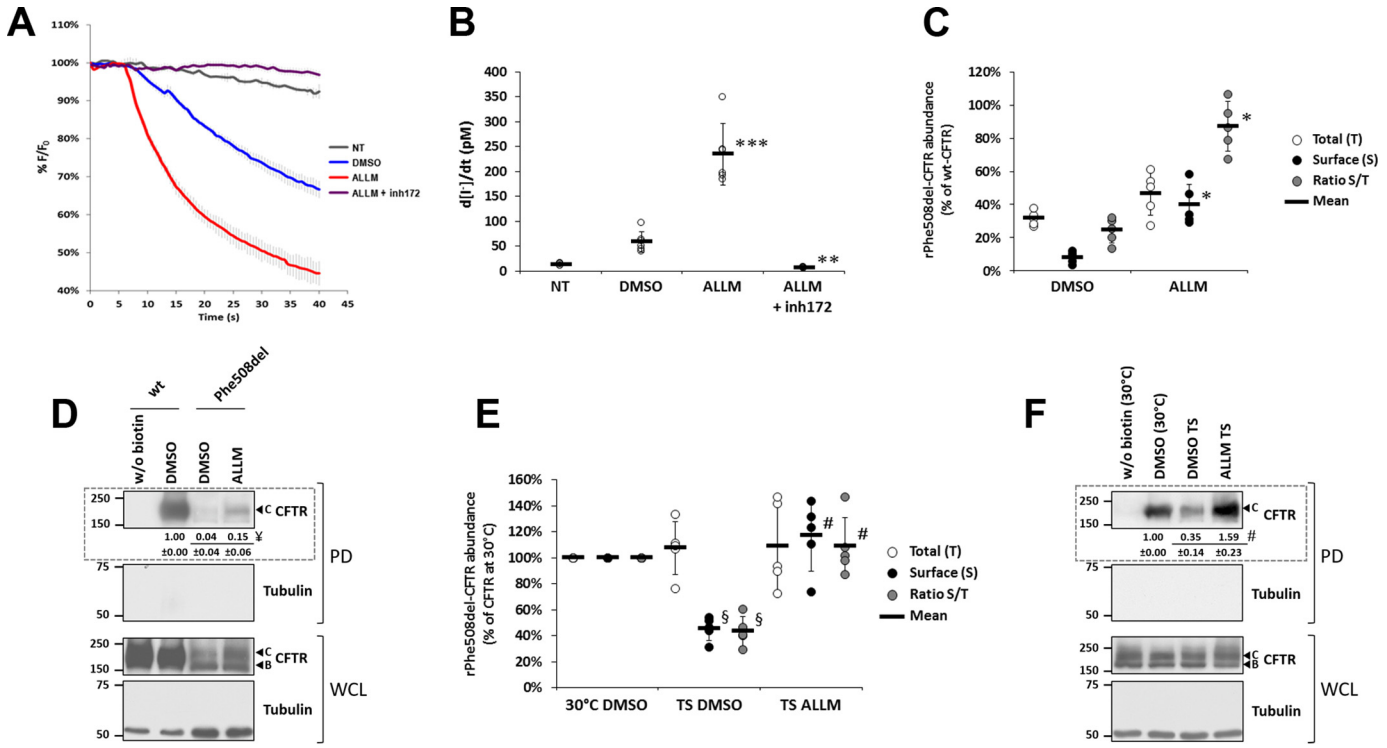

Figure 7. Chemical inhibition of CAPN1 increases rPhe508del-CFTR PM abundance, function, and stability. *A*, traces of iodide-induced HS-YFP fluorescence decay of CFBE Phe508del-CFTR cells treated with 3 μM VX-809 for 48 h, nontreated (*NT*) or co-treated with either DMSO or 250 nM ALLM CAPN1 inhibitor in the last 4 h, co-treated or not with 25 μM of inh172 for 15 min prior to stimulation for 30 min in PBS with Fsk and Gen, in the presence or absence of inh172, followed by continuous fluorescence recording and addition of I^-. *B*, summary of iodide influx rates calculated by fitting the iodide assay results to exponential decay curves. One-way ANOVA analysis detected significant differences between treatments ($F = 55.056$, $p < 0.001$). Post hoc Tukey's tests were used to identify significant variations relative to DMSO (***, $p < 0.001$) or ALLM (**, $p < 0.001$) alone. *C*, analysis of single-cell fluorescence signals in three independent experiments of Dox-induced mCherry-FLAG-wt- or Phe508del-CFTR cells, treated with 3 μM VX-809 for 48 h and co-treated with either DMSO or 250 nM ALLM CAPN1 inhibitor in the last 4 h. The data are presented as the means ± S.D. of total (*T*), surface (*S*), or *S*/*T* ratio of rPhe508del-CFTR abundance, expressed as percentages of wt-CFTR values. *D*, WB analysis of biotinylated cell surface proteins (biotin PD) and whole-cell lysates (*WCL*), treated as in *C*. *E*, analysis of single-cell fluorescence signals of Dox-induced mCherry–FLAG–Phe508del-CFTR cells, treated with 3 μM VX-809 for 48 h at 30 °C, and subjected to a TS of 4 h at 37 °C in the presence of either DMSO or 250 nM ALLM CAPN1 inhibitor, except for DMSO low temperature control (30 °C). The data are presented as total (*T*), surface (*S*), or *S*/*T* ratio of rPhe508del-CFTR abundance, expressed as percentages of CFTR at 30 °C (low temperature control). *F*, WB analysis of biotinylated cell surface proteins (biotin PD) and whole-cell lysates (*WCL*), treated as in *E*. The figure shows representative images and quantification results of five independent experiments. The means ± S.D. are given for all quantified data. The *dotted gray rectangles* in *D* and *F* highlight the respective quantification of CFTR abundance at the PM, relative to wt-CFTR with DMSO (*D*) and to DMSO at 30 °C (*F*). For *C*–*F*, significance was tested using unpaired, two-tailed *t* tests, comparing ALLM to DMSO (*C* and *D*; ¥, $p < 0.05$; *, $p < 0.001$), TS DMSO to 30 °C DMSO (*E*; §, $p < 0.001$), and TS ALLM to TS DMSO (*E* and *F*; #, $p < 0.001$).

teins should interact specifically with rPhe508del- but not with wt-CFTR, preventing EZR binding and causing rPhe508del-CFTR–NHERF1 destabilization at the PM. This hypothesis guided us to develop an assay to selectively IP and characterize CFTR-containing complexes from the PM. Notably, the whole CFTR interactome described by Pankow *et al.* (36) contained roughly one-third of the interactors identified by our PM-directed analysis. This is consistent with a compartment-specific enrichment of our data set, supporting the selectivity of the experimental approach used here. Our hypothesis also guided the bioinformatic analysis of the gathered data, allowing us to converge our MS data set from a network of 532 putative interactors to a subnetwork of 22 core proteins with a high probability to interact directly with rPhe508del-CFTR–NHERF1 complexes at the PM. Among these high confidence-scoring proteins, CAPN1 stood out as a potentially druggable candidate, because chemical inhibitors for this protein were already described. Of note, this does not exclude that several other relevant regulators of CFTR PM stability may exist among the many identified interactors, leaving an open door for further studies of these additional candidate proteins.

Notwithstanding, we showed here that CAPN1, a ubiquitous cytoskeleton- and PM-associated Ca^{2+}-dependent cysteine protease (43), is present within the PM complex assembled around rPhe508del-CFTR, but not around wt-CFTR proteins. Moreover, we demonstrated that chemical inhibition of CAPN1 with ALLM promotes the PM stabilization of VX-809–rPhe508del-CFTR in bronchial epithelial cells, leading to a near 4-fold increase in the functional restoration of CFTR-mediated ion transport. Although ALLM has a higher specificity to inhibit CAPN1 over other calpains, it is also an effective inhibitor of cathepsins, a group of lysosome-associated proteases (51). Because degradation of rPhe508del-CFTR internalized from the PM was described to occur mainly at the lysosome compartment (41), we cannot exclude a partial contribution of cathepsin inhibition to the increased PM levels of rPhe508del-CFTR upon ALLM treatment. Indeed, whereas siRNA-mediated CAPN1 knockdown produced a similar effect to ALLM treatment regarding PM abundance, stability, and functional rescue of Phe508del-CFTR, the overall magnitude of the effect was lower under siRNA than that achieved with the chemical inhibitor. Previous studies in PBMCs of patients

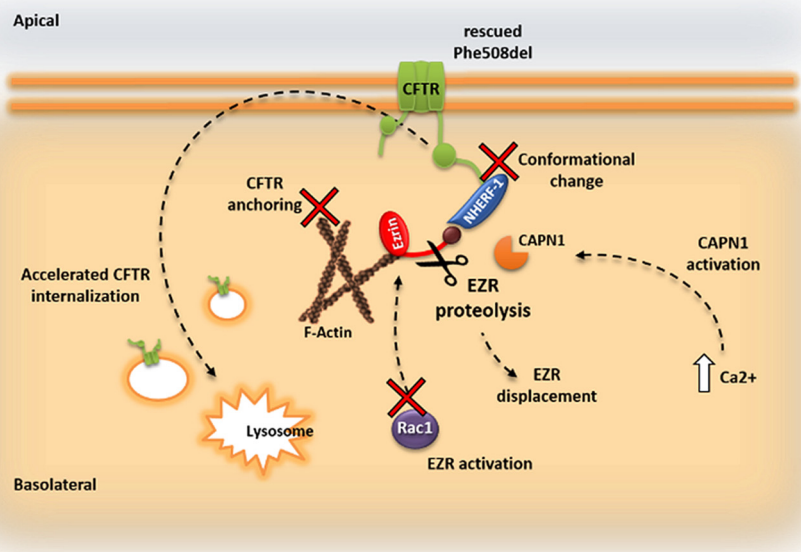

Figure 8. Scheme of the proposed mechanism by which CAPN1 affects rPhe508del-CFTR PM abundance and retention. See text for details.

homozygous for Phe508del-CFTR showed that elevated levels of intracellular Ca^{2+} led to an unbalance in the calpain/calpastatin system, resulting in a constitutive CAPN1 activation caused by a decrease in their specific inhibitory regulators, leading to a reduction of mature CFTR in PBMCs (44). These authors also showed that CAPN1 activity could compromise CFTR function by targeting CFTR–NHERF1 complexes at the PM and that total EZR protein levels were lower in the PBMC of CF patients (44). Although the expression of CFTR in PBMCs is still subject to controversy (61, 62), Ca^{2+} was also found elevated in epithelial airway cells of CF patients (63–66), suggesting a similar up-regulation of CAPN1 activity in these cells. Moreover, whereas the authors did not fully elucidate the mechanism of PM CFTR destabilization in PBMCs (44), here we show that knockdown of CAPN1 stabilizes Phe508del-CFTR by promoting the association of endogenous EZR with the CFTR–NHERF1 complex at the PM. This result is consistent with our previous findings showing that it is possible to coax the anchoring and PM retention of chemically rescued Phe508del-CFTR by promoting the activation and association of EZR to CFTR–NHERF1 complexes at the PM, by increasing endogenous RAC1 signaling through the stimulation of airway epithelial cells with HGF (28, 42). The binding of activated EZR induces a conformational change in NHERF1 exposing a second PDZ domain for CFTR binding, which stabilizes the rescued channel at the cell surface, leading to a 3-fold increase in the functional restoration achieved by corrector drugs, such as VX-809 (28, 29, 42). An equivalent extent of functional recovery was observed with CAPN1 inhibition, either by siRNA-mediated knockdown or by chemical inhibition with ALLM. These findings indicate that the proteolytic activity of CAPN1 is required for the destabilization of rPhe508del-CFTR at the PM. Consistently, EZR is among the known CAPN1 substrates, and remarkably, it is the only member of the ezrin–radixin–moesin (ERM) family to be cleaved by this protease *in vitro* (67). This supports an important function for CAPN1 in the regulation of EZR-mediated anchoring of PM proteins, namely CFTR.

All the gathered evidence led us to propose the following model (Fig. 8): elevated Ca^{2+} intracellular levels coupled to the recruitment of CAPN1 to rPhe508del-CFTR–NHERF1 PM complexes lead to the hydrolysis and displacement of EZR from the complex, preventing its activation by endogenous signaling events (such as those mediated by RAC1 (28)) and thus avoiding NHERF1 opening and the anchoring of rPhe508del-CFTR to the actin cytoskeleton. These events lead to the accelerated internalization and degradation of rescued channels, as described by us and others (19, 28, 29). Inhibition of CAPN1 allows the activation and binding of EZR to rPhe508del-CFTR–NHERF1 complexes at the PM, promoting the retention and thus stabilization of rescued channels at the cell surface.

Taken together, our results indicate that association of CAPN1 to the cell surface rPhe508del-CFTR–NHERF1 complexes plays an important role in reducing the half-life of rPhe508del-CFTR at the PM and that its pharmacological inhibition has a potentially relevant therapeutic application in combination therapies with other modulator drugs, namely correctors and potentiators. It should be noted that even though there are no CAPN1 inhibitors currently progressing into clinical trials, important advances are being made in their development, and several preclinical studies demonstrated their potential therapeutic value (68, 69). In accordance, further *in vivo* studies will now be required to evaluate the therapeutic applicability of CAPN1 inhibition for the benefit of people with CF disease.

Experimental procedures

Cell culture, treatment, and transfection

CFBE41o- cells stably transduced with lentivirus encoding mCherry–FLAG–tagged, wt- or Phe508del-CFTR under the Tet-ON promoter were generated by Adv Bioscience LLC as

described before (70). A clone of CFBE stably expressing nontagged Phe508del-CFTR cell(45) was modified to stably co-express the halide sensor YFP–F46L/H148Q/I152L (HS-YFP, a gift from P. Haggie, University of California, San Francisco, School of Medicine).

All cell lines were reversed transfected as described in Ref. 39 and cultured in minimum essential medium supplemented with GlutaMAX, Earle's salts, 10% (v/v) heat-inactivated fetal bovine serum, and 2 μg/ml puromycin (all from Thermo Fisher Scientific) at 37 °C with 5% CO_2. mCherry-FLAG-CFTR cells were additionally selected with 10 mg/ml blasticidin (Santa Cruz Biotechnology), whereas the cells expressing the HS-YFP were selected with 0.4 mg/ml hygromycin B (Thermo Fisher Scientific). The cells were transfected with Lipofectamine 2000 (Thermo Fisher Scientific) in 35-mm dishes with 220 pmol of the indicated siRNAs and analyzed at the indicated time points. The siRNA oligonucleotide control against luciferase (siLuc, 5′-CGUACGCGGAAUACUUCGA) was from Eurofins Genomics, and the triple oligonucleotide mix against calpain 1 (sc-29885) was from Santa Cruz Biotechnology. Stock solutions of Fsk (10 mM, Sigma–Aldrich), Gen (50 mM, Sigma–Aldrich), CFTR-specific inhibitor 172 (inh172, 10 mM, CFFT USA), VX-809 (10 mM, Gentaur), and ALLM (5 mg/ml, Merck Millipore) were prepared in DMSO.

SDS-PAGE and immunoblotting

Total protein was quantified by a modified micro-Lowry method, and 30 μg of total protein was loaded and separated on 9% (w/v) SDS-PAGE gels with 1% (v/v) glycerol. For detection of specific proteins, SDS-PAGE gels were transferred onto polyvinylidene difluoride membranes (Bio-Rad). WB membranes were blocked in TBS + 0.1% (v/v) Triton X-100 + 5% (w/v) milk and probed using the following primary antibodies: mouse anti-CFTR clone 596 (CFFT USA); goat anti-CAPN1 clone N-19 (sc-7531, Santa Cruz Biotechnology); mouse anti-EZR clone 1E11 (SAB1402391, Sigma–Aldrich); mouse anti-NHERF-1 clone A7 (sc-271552, Santa Cruz Biotechnology); rabbit anti-PDIA3 (HPA003230, Sigma–Aldrich); rabbit anti–GLUT-1 (Ab652, Abcam); and mouse anti–α-tubulin clone B-5–1-2 (T5168, Sigma–Aldrich). For densitometry analysis of WB bands, x-rays films were digitalized, and the images were analyzed with ImageJ software (National Institutes of Health).

Co-immunoprecipitation of membrane CFTR-associated complexes

CFBE mCherry-FLAG-wt-CFTR cells were incubated at 37 °C for 48 h after Dox-induced CFTR expression (1 μg/ml, Sigma–Aldrich), whereas CFBE mCherry–FLAG–Phe508del-CFTR cells were incubated in three different conditions for 48 h after Dox-induced CFTR expression: at 37 °C; at 26 °C for lower temperature CFTR correction; and at 30 °C with VX-809 mediated pharmacological correction (5 μM, Gentaur). For each condition, cells near confluence on 100-mm culture dishes were gently, but thoroughly, washed with ice-cold PBS-CM. The cells were then placed on ice, rinsed three times, and left 5 min in cold PBS-CM to ensure arrest of endocytic traffic. The cells were incubated with soft agitation for 2 h with anti-FLAG M2 Ab (F3165, Sigma–Aldrich)—all dishes except one, used as no Ab control—and rinsed three times with ice-cold PBS-CM. Each condition was incubated with the cross-link solution dithiobis (succinimidyl propionate) + succinimidyl 3-(2-pyridyldithio)propionate (1:1, 0.2 mM, Thermo Fisher Scientific) for 2 h with soft agitation, rinsed twice, and left for 15 min with Tris-HCl (50 mM Tris-HCl, pH 7.5) to quench the reaction. The cells were again washed three times with cold PBS-CM and lysed in 500 μl of lysis buffer (50 mM Tris-HCl, pH 7.5, 2 mM $MgCl_2$, 100 mM NaCl, 10% (v/v) glycerol, 1% (v/v) Nonidet P-40, 0.01% (v/v) SDS, Protease inhibitor mixture; Sigma). Cell lysates were first cleared at 3100 × *g* for 5 min at 4 °C. ~450 μl of lysate were added to 45 μl of streptavidin–agarose beads (Sigma–Aldrich,) to further clear the lysates and were rotated for 1 h at 4 °C, centrifuged for 1 min at 3100 × *g*, and recovered. ~400 μl of the cleared lysates were added to 40 μl of G-protein–agarose beads (Roche), rotated for 1 h at 4 °C, centrifuged for 1 min at 3100 × *g*, and washed six times in cold wash buffer (50 mM Tris-HCl, pH 7.5, 2 mM $MgCl_2$, 300 mM NaCl, 10% (v/v) glycerol, 1% (v/v) Nonidet P-40, 0.1% (v/v) SDS). Captured proteins were recovered in 50 μl of 2× sample buffer with DTT (100 mM).

MS-compatible silver staining and nano-LC MS/MS

Captured membrane CFTR-associated protein complexes were separated on 9% (w/v) SDS-PAGE gels and run for 1 cm. The gels were then silver-stained through a MS-compatible protocol, as described in Ref. 40. Briefly, the gels were transferred to a glass tray and fixed for 1 h at room temperature in fixer solution (40% ethanol, 10% glacial acetic acid, 50% ddH_2O), and washed overnight in ddH_2O. The gels were sensitized in 0.02% sodium thiosulfate for 1 min and washed tree times with ddH_2O. The gels were then incubated in cold 0.1% silver nitrate solution with 0.02% formaldehyde (added just before use) for 20 min and washed twice with ddH_2O. The gels were transferred to a new tray and washed for 1 min before developing in 3% sodium carbonate solution, with 0.05% formaldehyde (added just before use) until distinct bands were visible. After ddH_2O washing, staining was fixed in 5% acetic acid for 5 min, and the gels were stored at 4 °C in 1% acetic acid until MS analysis. For MS analysis, the entire 1-cm lanes corresponding to each sample run were excised from the gels and sent in ddH_2O for nano-LC MS/MS analysis on a SCIEX TripleTOF 6600 system, outsourced to UniMS (Instituto de Tecnologia Química e Biológica António Xavier Institute, Oeiras, Portugal).

Nano-LC-MS/MS analyses

Nano-LC–MS/MS analysis was performed on an ekspert™ Nano-LC 425 cHiPLC® system coupled with a TripleTOF® 6600 with a NanoSpray® III source (Sciex). Peptides were separated through reversed-phase LC in a trap-and-elute mode. Trapping was performed at 2 μl/min on a Nano cHiPLC Trap column (Sciex 200 μm × 0.5 mm, ChromXP C18-CL, 3 μm, 120 Å) with 100% A (0.1% formic acid) for 10 min. The separation was performed at 300 nl/min, on a Nano cHiPLC column (Sciex 75 μm × 15 cm, ChromXP C18-CL, 3 μm, 120 Å). The gradient was as follows: 0–1 min, 5% B (0.1% formic acid in acetonitrile, Fisher Chemicals); 1–91 min, 5–30% B; 91–93 min,

30–80% B; 93–108 min, 80% B; 108–110 min, 80–5% B; and 110–127 min, 5% B. The peptides were sprayed into the MS through an uncoated fused-silica PicoTip™ emitter (360-μm outer diameter, 20-μm inner diameter, 10 ± 1.0-μm tip inner diameter; New Objective). The source parameters were set as follows: 15 ion source gas 1, 0 ion source gas 2, 30 curtain gas, 2.5 keV ion spray voltage floating, and 100 °C interface heater temperature. An information-dependent acquisition method was set with a TOF–MS survey scan of 400–2000 m/z. The 50 most intense precursors were selected for subsequent fragmentation, and the MS/MS were acquired in high sensitivity mode for 40 ms. The obtained spectra were processed and analyzed using ProteinPilot™ software, with the Paragon search engine (version 5.0, Sciex). A UniProt TrEMBL database (20422 entries, accessed in 29 April 2015) containing the sequences of the proteins from the organism *Homo sapiens* (Taxon ID: 9606) was used. The following search parameters were set: iodoacetamide, as Cys alkylation; trypsin, as digestion; TripleTOF 6600, as the instrument; ID focus as biological modifications and amino acid substitutions; search effort as thorough; and an false discovery rate analysis. Based on the data set size, the false discovery rate was determined to be below 5% for proteins with a calculated unused protein score (ProteinPilot™ software) above 1.3 (95% confidence).

Bioinformatics analyses of MS data

Confidence in protein detection

Precipitation of CFTR membrane association complex was performed in three replicates. In each replicate, identification of each protein in MS spectra was characterized by a PCS, detected with ProteinPilot™ Software (Sciex). For PCS of >1.3, the confidence in the identification of that particular protein in the sample is equal or higher than 95%. To conjugate this individual score with the detection of the same protein across replicates, we generated a CCS, defined by five levels of confidence for protein detection: level 5 proteins are detected with PCS ≥ 1.3 in more than one replicate and not in the controls; level 4 proteins are detected in one replicate with PCS ≥ 1.3 and not in the controls; level 3 proteins are detected in more replicates than in controls and with an average PCS higher than their respective the controls; level 2 proteins are detected in one replicate with PCS ≤ 1.3 and not in the controls; and level 1 proteins are detected in the same number of replicates and controls, with a replicate average PCS higher than the corresponding controls. All other cases are included in level 0, where proteins are not considered to be consistently present in the set of replicates.

Human interactome network

Interactions between detected proteins were retrieved from a human interactome network, built from two data sources: Agile Protein Interactomes DataServer and the Human Reference Protein Interactome Mapping Project (http://interactome.baderlab.org).[3] APID collects physical protein interactions reported in the literature. We used all the interactions available in APID between human proteins. The Human Reference Protein Interactome Mapping Project gives access to interactions detected through unbiased high-throughput pairwise protein interaction experimental detection. Network analyses were conducted in *R* using functions from the iGraph package. Network visualizations were produced with Cytoscape.

CFTR–EZR–NHERF1 interaction interference score

To measure the capability of individual proteins to interfere with the formation of the interactions between CFTR–EZR–NHERF1, we developed a quantitative score. First, for a given subnetwork containing these three proteins, the number of paths linking two of these proteins through two, three, or four interactions (path length) is computed. For each protein in the network it is determined the fraction of paths of each length that pass through its node. The final score is a weighted sum of these fractions, where fractions associated with higher lengths have lower weights (Equation 1).

$$\text{Score} = (\%\ \text{path length 2}) + 0.5 \times (\%\ \text{path length 3}) + 0.25 \times (\%\ \text{path length 4}) \quad \text{(Eq. 1)}$$

Validation of hit proteins by co-IP of PM CFTR-associated proteins

CFBE mCherry-FLAG-wt and Phe508del-CFTR cells were incubated at 37 °C for 48 h after Dox-induced CFTR expression (1 μg/ml, Sigma–Aldrich), with mCherry–FLAG–Phe508del-CFTR cells being additionally treated with VX-809 (3 μM, Gentaur). For both conditions, the cells were placed on ice, washed three times with ice-cold PBS-CM, and left for 5 min in cold PBS-CM. The cells were then incubated with soft agitation for 2 h with anti-FLAG M2 Ab (F3165, Sigma–Aldrich) and rinsed three times with ice-cold PBS-CM. No cross-linking agents were used. The cells were then lysed in 500 μl of lysis buffer, and lysates were processed as described under "Co-immunoprecipitation of membrane CFTR-associated complexes." Captured proteins were analyzed by SDS-PAGE and immunoblotting (see *SDS-PAGE and immunoblotting*) with the indicated antibodies.

Immunofluorescence and confocal microscopy

CFBE mCherry-FLAG-wt and Phe508del-CFTR cells, grown on coverslips, were induced with Dox (1 μg/ml, Sigma–Aldrich) and treated as indicated. Afterward, the cells were rinsed on ice with cold PBS-CM (PBS, pH 8.0, containing 0.1 mM $CaCl_2$ and 1 mM $MgCl_2$) and incubated with anti-FLAG M2 Ab (F3165, Sigma–Aldrich) in PBS-CM for 1 h at 4 °C, without permeabilization. The cells were washed three times with ice-cold PBS-CM and incubated with anti-mouse Alexa Fluor 488 secondary Ab (Thermo Fisher Scientific) for 1 h at 4 °C. The cells were again thoroughly washed in PBS and then fixed with 4% formaldehyde for 15 min, stained with 4′,6-diamidino-2-phenylindole (DAPI), and mounted on microscope slides with Vectashield (Vector Laboratories). Images were acquired on a Leica TCS-SPE confocal microscope.

Biotinylation of cell surface proteins

CFBE mCherry-FLAG-wt and Phe508del-CFTR cells were induced with Dox (1 μg/ml, Sigma–Aldrich) and treated as

indicated. Afterward, the 0cells were placed on ice, washed three times with ice-cold PBS-CM, and left for 5 min in cold PBS-CM. The cells were then incubated for 45 min with 0.5 mg of EZ-Link Sulfo-NHS-SS-Biotin (Santa Cruz Biotechnology) to label all cell surface proteins. The cells were rinsed twice and then left for 15 min on ice with ice-cold Tris-Q (100 mM Tris-HCl, pH 8.0, 150 mM NaCl, 0.1 mM $CaCl_2$, 1 mM $MgCl_2$, 10 mM glycine, 1% (w/v) BSA) to quench the reaction. The cells were again washed three times with cold PBS-CM and lysed in 250 μl of pulldown (PD) buffer (50 mM Tris-HCl, pH 7.5, 100 mM NaCl, 10% (v/v) glycerol, 1% (v/v) Nonidet P-40, Protease inhibitor mixture; Sigma–Aldrich). The cell lysates were cleared at 7000 $\times$ *g* for 5 min at 4 °C, and an aliquot of 40 μl, representing input CFTR levels, was removed, whereas 200 μl of lysate were added to 20 μl of G-protein–agarose beads (Roche) to further clear the lysates. These were rotated for 1 h at 4 °C, centrifuged for 1 min at 3100 $\times$ *g*, and recovered. The cleared lysates were added to 20 μl of streptavidin–agarose beads (Sigma–Aldrich), previously incubated for 1 h in 1 ml of cold pulldown buffer containing 2% (w/v) milk, and washed three times in PD buffer. Lysate and beads were rotated for 1 h at 4 °C, centrifuged for 1 min at 3100 $\times$ *g*, and washed five times in cold wash buffer (100 mM Tris-HCl, pH 7.5, 300 mM NaCl, 1% (v/v) Triton X-100). Captured proteins were recovered in 20 μl of 2$\times$ sample buffer with 100 mM DTT and analyzed by SDS-PAGE and immunoblotting, as described above.

Protein thermal destabilization assay (TS assay)

CFBE mCherry–FLAG–Phe508del-CFTR cells were induced with Dox (1 μg/ml, Sigma–Aldrich) and incubated for 48 h at 30 °C with VX-809 (3 μM, Gentaur). These conditions were previously optimized to achieve rPhe508del-CFTR PM levels near to those of wt-CFTR (29). The cells were next transferred to 37 °C for 4 h to destabilize the rPhe508del-CFTR at the PM, as described in Ref. 41. The cells were then placed on ice, washed three times with ice-cold PBS-CM, and left 5 min in cold PBS-CM. The cells were then analyzed by confocal immune fluorescence or biotinylation of surface proteins, as described above.

CFTR functional assay by HS-YFP

CFBE Phe508del-CFTR cells constitutively expressing HS-YFP-F46L/H148Q/I152L (45) were seeded in 8-well chamber slides and treated as described. The cells were then carefully washed twice with isomolar PBS (WPBS: 137 mM NaCl, 2.7 mM KCl, 0.7 mM $CaCl_2$, 1.1 mM $MgCl_2$, 1.5 mM KH_2PO_4, 8.1 mM Na_2HPO_4, pH 7.4) and incubated for 30 min with WPBS containing compounds for CFTR stimulation/inhibition (5 μM Fsk, 20 μM Gen, and 25 μM inh172, all from Sigma–Aldrich), as indicated. The slides were then transferred to a Leica TCS-SPE confocal microscope for time-lapse analysis. Each well was assayed individually for iodide influx by recording fluorescence continuously (500 ms/point) for 5 s (baseline) and then for 35 s after the rapid ($\leq$1 s) addition of isomolar PBS in which 137 mM Cl^- was replaced by I^- (final NaI concentration of 100 mM/plate well). The cells were kept at 37 °C up until being assayed at room temperature. After background subtraction, HS-YFP fluorescence recordings (*F*) were normalized to the initial average value measured before addition of I^- (F_0). Quantification of fluorescence decay was performed on at least 24 individual cells/well, using ImageJ (National Institutes of Health) as previously described (42). The average fluorescence decay was fitted to an exponential decay function to derive the maximal slope that corresponds to initial influx of I^- into the cells. Maximal slopes were converted into I^- variation rates (in nM/s) using the equation $d[I^-]/d_t = K_d\,[d(F/F_0)/d_t]$, where K_d is the affinity constant of YFP for I^- (29).

Statistical analyses

Statistical analysis was performed using GraphPad Prism 5 software. The quantitative results are shown as means $\pm$ S.E. of at least three independent experiments. To compare sets of data, we used either one-way ANOVA followed by Tukey's test (for multiple treatments) or two tailed Student's *t* tests (comparison between two treatments) and considered significant differences when p values < 0.05.

Author contributions—A. M. M., P. B., and P. M. validation; A. M. M. and P. B. investigation; A. M. M. and F. R. P. methodology; A. M. M. and P. M. writing-original draft; F. R. P. software; F. R. P. and P. M. formal analysis; F. R. P., P. B., M. D. A., and R. P. writing-review and editing; M. D. A. and P. M. resources; M. D. A. and P. M. funding acquisition; R. P. and P. M. supervision; P. M. conceptualization; P. M. project administration.

Acknowledgment—We acknowledge Dr. P. Haggie (University of California, San Francisco, School of Medicine) for the kind gift of halide-sensitive YFP-F46L/H148Q/I152L plasmid.

References

1. Riordan, J. R., Rommens, J. M., Kerem, B., Alon, N., Rozmahel, R., Grzelczak, Z., Zielenski, J., Lok, S., Plavsic, N., and Chou, J. L. (1989) Identification of the cystic fibrosis gene: cloning and characterization of complementary DNA. *Science* **245,** 1066–1073 CrossRef Medline
2. Sosnay, P. R., Siklosi, K. R., Van Goor, F., Kaniecki, K., Yu, H., Sharma, N., Ramalho, A. S., Amaral, M. D., Dorfman, R., Zielenski, J., Masica, D. L., Karchin, R., Millen, L., Thomas, P. J., Patrinos, G. P., *et al.* (2013) Defining the disease liability of variants in the cystic fibrosis transmembrane conductance regulator gene. *Nat. Genet.* **45,** 1160–1167 CrossRef Medline
3. Huang, D. W, Sherman, B. T., and Lempicki, R. A. (2009) Systematic and integrative analysis of large gene lists using DAVID bioinformatics resources. *Nat. Protoc.* **4,** 44–57 CrossRef Medline
4. De Boeck, K., Zolin, A., Cuppens, H., Olesen, H. V., and Viviani, L. (2014) The relative frequency of CFTR mutation classes in European patients with cystic fibrosis. *J. Cyst. Fibros.* **13,** 403–409 CrossRef Medline
5. Carvalho-Oliveira, I., Efthymiadou, A., Malhó, R., Nogueira, P., Tzetis, M., Kanavakis, E., Amaral, M. D., and Penque, D. (2004) CFTR localization in native airway cells and cell lines expressing wild-type or F508del-CFTR by a panel of different antibodies. *J. Histochem. Cytochem.* **52,** 193–203 CrossRef Medline
6. Farinha, C. M., Matos, P., and Amaral, M. D. (2013) Control of cystic fibrosis transmembrane conductance regulator membrane trafficking: not just from the endoplasmic reticulum to the Golgi. *FEBS J.* **280,** 4396–4406 CrossRef Medline
7. Farinha, C. M., and Canato, S. (2017) From the endoplasmic reticulum to the plasma membrane: mechanisms of CFTR folding and trafficking. *Cell. Mol. Life Sci.* **74,** 39–55 CrossRef Medline
8. Bronsveld, I., Mekus, F., Bijman, J., Ballmann, M., Greipel, J., Hundrieser, J., Halley, D. J., Laabs, U., Busche, R., De Jonge, H. R., Tümmler, B., and Veeze, H. J. (2000) Residual chloride secretion in intestinal tissue of del-

taF508 homozygous twins and siblings with cystic fibrosis: the European CF Twin and Sibling Study Consortium. *Gastroenterology* **119,** 32–40 CrossRef Medline

9. Kälin, N., Claass, A., Sommer, M., Puchelle, E., and Tümmler, B. (1999) ΔF508 CFTR protein expression in tissues from patients with cystic fibrosis. *J. Clin. Invest.* **103,** 1379–1389 CrossRef Medline
10. Swiatecka-Urban, A., Brown, A., Moreau-Marquis, S., Renuka, J., Coutermarsh, B., Barnaby, R., Karlson, K. H., Flotte, T. R., Fukuda, M., Langford, G. M., and Stanton, B. A. (2005) The short apical membrane half-life of rescued ΔF508-cystic fibrosis transmembrane conductance regulator (CFTR) results from accelerated endocytosis of ΔF508-CFTR in polarized human airway epithelial cells. *J. Biol. Chem.* **280,** 36762–36772 CrossRef Medline
11. Heda, G. D., Tanwani, M., and Marino, C. R. (2001) The Delta F508 mutation shortens the biochemical half-life of plasma membrane CFTR in polarized epithelial cells. *Am. J. Physiol. Cell Physiol.* **280,** C166–C174 CrossRef Medline
12. Matos, A. M., and Matos, P. (2018) Combination therapy in Phe508del CFTR: how many will be enough? *J. Lung Health Dis.* **2,** 9–16
13. Bell, S. C., De Boeck, K., and Amaral, M. D. (2015) New pharmacological approaches for cystic fibrosis: promises, progress, pitfalls. *Pharmacol. Ther.* **145,** 19–34 CrossRef Medline
14. Grasemann, H. (2017) CFTR modulator therapy for cystic fibrosis. *N. Engl. J. Med.* **377,** 2085–2088 CrossRef Medline
15. Huang, D. W., Sherman, B. T., and Lempicki, R. A. (2009) Bioinformatics enrichment tools: Paths toward the comprehensive functional analysis of large gene lists. *Nucleic Acids Res.* **37,** 1–13 CrossRef Medline
16. Van Goor, F., Hadida, S., Grootenhuis, P. D., Burton, B., Stack, J. H., Straley, K. S., Decker, C. J., Miller, M., McCartney, J., Olson, E. R., Wine, J. J., Frizzell, R. A., Ashlock, M., and Negulescu, P. A. (2011) Correction of the F508del-CFTR protein processing defect *in vitro* by the investigational drug VX-809. *Proc. Natl. Acad. Sci. U.S.A.* **108,** 18843–18848 CrossRef Medline
17. Ren, H. Y., Grove, D. E., De La Rosa, O., Houck, S. A., Sopha, P., Van Goor, F., Hoffman, B. J., and Cyr, D. M. (2013) VX-809 corrects folding defects in cystic fibrosis transmembrane conductance regulator protein through action on membrane-spanning domain 1. *Mol. Biol. Cell.* **24,** 3016–3024 CrossRef Medline
18. Farinha, C. M., King-Underwood, J., Sousa, M., Correia, A. R., Henriques, B. J., Roxo-Rosa, M., Da Paula, A. C., Williams, J., Hirst, S., Gomes, C. M., and Amaral, M. D. (2013) Revertants, low temperature, and correctors reveal the mechanism of F508del-CFTR rescue by VX-809 and suggest multiple agents for full correction. *Chem. Biol.* **20,** 943–955 CrossRef Medline
19. Okiyoneda, T., Veit, G., Dekkers, J. F., Bagdany, M., Soya, N., Xu, H., Roldan, A., Verkman, A. S., Kurth, M., Simon, A., Hegedus, T., Beekman, J. M., and Lukacs, G. L. (2013) Mechanism-based corrector combination restores ΔF508-CFTR folding and function. *Nat. Chem. Biol.* **9,** 444–454 CrossRef Medline
20. Ramsey, B. W., Davies, J., McElvaney, N. G., Tullis, E., Bell, S. C., Dřevínek, P., Griese, M., McKone, E. F., Wainwright, C. E., Konstan, M. W., Moss, R., Ratjen, F., Sermet-Gaudelus, I., Rowe, S. M., Dong, Q., *et al.* (2011) A CFTR potentiator in patients with cystic fibrosis and the *G551D* mutation. *N. Engl. J. Med.* **365,** 1663–1672 CrossRef Medline
21. Wainwright, C. E., Elborn, J. S., Ramsey, B. W., Marigowda, G., Huang, X., Cipolli, M., Colombo, C., Davies, J. C., De Boeck, K., Flume, P. A., Konstan, M. W., McColley, S. A., McCoy, K., McKone, E. F., Munck, A., *et al.* (2015) Lumacaftor–ivacaftor in patients with cystic fibrosis homozygous for Phe508del CFTR. *N. Engl. J. Med.* **373,** 220–231 CrossRef Medline
22. Clancy, J. P., Rowe, S. M., Accurso, F. J., Aitken, M. L., Amin, R. S., Ashlock, M. A., Ballmann, M., Boyle, M. P., Bronsveld, I., Campbell, P. W., De Boeck, K., Donaldson, S. H., Dorkin, H. L., Dunitz, J. M., Durie, P. R., *et al.* (2012) Results of a phase IIa study of VX-809, an investigational CFTR corrector compound, in subjects with cystic fibrosis homozygous for the F508del-CFTR mutation. *Thorax* **67,** 12–18 CrossRef Medline
23. Boyle, M. P., Bell, S. C., Konstan, M. W., McColley, S. A., Rowe, S. M., Rietschel, E., Huang, X., Waltz, D., Patel, N. R., Rodman, D., and VX09-809-102 Study Group (2014) A CFTR corrector (lumacaftor) and a CFTR potentiator (ivacaftor) for treatment of patients with cystic fibrosis who have a Phe508del CFTR mutation: a phase 2 randomised controlled trial. *Lancet Respir. Med.* **2,** 527–538 Medline
24. Elborn, J. S., Ramsey, B. W., Boyle, M. P., Konstan, M. W., Huang, X., Marigowda, G., Waltz, D., Wainwright, C. E., and VX-809 TRAFFIC and TRANSPORT Study Groups (2016) Efficacy and safety of lumacaftor/ivacaftor combination therapy in patients with cystic fibrosis homozygous for Phe508del CFTR by pulmonary function subgroup: a pooled analysis. *Lancet Respir. Med.* **4,** 617–626 CrossRef Medline
25. Donaldson, S. H., Pilewski, J. M., Griese, M., Cooke, J., Viswanathan, L., Tullis, E., Davies, J. C., Lekstrom-Himes, J. A., Wang, L. T., and VX11-661-101 Study Group (2018) Tezacaftor/ivacaftor in subjects with cystic fibrosis and F508del/F508del-CFTR or F508del/G551D-CFTR. *Am. J. Respir. Crit. Care Med.* **197,** 214–224 CrossRef Medline
26. Taylor-Cousar, J. L., Munck, A., McKone, E. F., van der Ent, C. K., Moeller, A., Simard, C., Wang, L. T., Ingenito, E. P., McKee, C., Lu, Y., Lekstrom-Himes, J., and Elborn, J. S. (2017) Tezacaftor–ivacaftor in patients with cystic fibrosis homozygous for Phe508del. *N. Engl. J. Med.* **377,** 2013–2023 CrossRef Medline
27. Rowe, S. M., Daines, C., Ringshausen, F. C., Kerem, E., Wilson, J., Tullis, E., Nair, N., Simard, C., Han, L., Ingenito, E. P., McKee, C., Lekstrom-Himes, J., and Davies, J. C. (2017) Tezacaftor–ivacaftor in residual-function heterozygotes with cystic fibrosis. *N. Engl. J. Med.* **377,** 2024–2035 CrossRef Medline
28. Moniz, S., Sousa, M., Moraes, B. J., Mendes, A. I., Palma, M., Barreto, C., Fragata, J. I., Amaral, M. D., and Matos, P. (2013) HGF stimulation of Rac1 signaling enhances pharmacological correction of the most prevalent cystic fibrosis mutant F508del-CFTR. *ACS Chem. Biol.* **8,** 432–442 CrossRef Medline
29. Loureiro, C. A., Matos, A. M., Dias-Alves, Â., Pereira, J. F., Uliyakina, I., Barros, P., Amaral, M. D., and Matos, P. (2015) A molecular switch in the scaffold NHERF1 enables misfolded CFTR to evade the peripheral quality control checkpoint. *Sci. Signal.* **8,** ra48 CrossRef Medline
30. Keating, D., Marigowda, G., Burr, L., Daines, C., Mall, M. A., McKone, E. F., Ramsey, B. W., Rowe, S. M., Sass, L. A., Tullis, E., McKee, C. M., Moskowitz, S. M., Robertson, S., Savage, J., Simard, C., *et al.* (2018) VX-445–tezacaftor–ivacaftor in patients with cystic fibrosis and one or two Phe508del alleles. *N. Engl. J. Med.* **379,** 1612–1620 CrossRef Medline
31. Davies, J. C., Moskowitz, S. M., Brown, C., Horsley, A., Mall, M. A., McKone, E. F., Plant, B. J., Prais, D., Ramsey, B. W., Taylor-Cousar, J. L., Tullis, E., Uluer, A., McKee, C. M., Robertson, S., Shilling, R. A., *et al.* (2018) VX-659–tezacaftor–ivacaftor in patients with cystic fibrosis and one or two Phe508del alleles. *N. Engl. J. Med.* **379,** 1599–1611 CrossRef Medline
32. Li, C., and Naren, A. P. (2010) CFTR chloride channel in the apical compartments: spatiotemporal coupling to its interacting partners. *Integr. Biol.* (*Camb.*) **2,** 161–177 Medline
33. Li, C., and Naren, A. P. (2005) Macromolecular complexes of cystic fibrosis transmembrane conductance regulator and its interacting partners. *Pharmacol. Ther.* **108,** 208–223 CrossRef Medline
34. Kunzelmann, K. (2001) CFTR: interacting with everything? *News Physiol. Sci.* **16,** 167–170 Medline
35. Wang, S., and Li, M. (2001) Molecular studies of CFTR interacting proteins. *Pflugers Arch.* **443,** S62–S64 CrossRef Medline
36. Pankow, S., Bamberger, C., Calzolari, D., Martínez-Bartolomé, S., Lavallée-Adam, M., Balch, W. E., and Yates, J. R., 3rd (2015) ΔF508 CFTR interactome remodelling promotes rescue of cystic fibrosis. *Nature* **528,** 510–516 CrossRef Medline
37. Kristensen, A. R., Gsponer, J., and Foster, L. J. (2012) A high-throughput approach for measuring temporal changes in the interactome. *Nat. Methods.* **9,** 907–909 CrossRef Medline
38. Fukuda, R., and Okiyoneda, T. (2018) Peripheral protein quality control as a novel drug target for CFTR stabilizer. *Front. Pharmacol.* **9,** 1100 CrossRef Medline
39. Botelho, H. M., Uliyakina, I., Awatade, N. T., Proença, M. C., Tischer, C., Sirianant, L., Kunzelmann, K., Pepperkok, R., and Amaral, M. D. (2015) Protein traffic disorders: an effective high-throughput fluorescence microscopy pipeline for drug discovery. *Sci. Rep.* **5,** 9038 CrossRef Medline

40. Shevchenko, A., Wilm, M., Vorm, O., and Mann, M. (1996) Mass spectrometric sequencing of proteins from silver-stained polyacrylamide gels. *Anal. Chem.* **68,** 850–858 CrossRef Medline
41. Okiyoneda, T., Barrière, H., Bagdány, M., Rabeh, W. M., Du, K., Höhfeld, J., Young, J. C., and Lukacs, G. L. (2010) Peripheral protein quality control removes unfolded CFTR from the plasma membrane. *Science* **329,** 805–810 CrossRef Medline
42. Matos, A. M., Gomes-Duarte, A., Faria, M., Barros, P., Jordan, P., Amaral, M. D., and Matos, P. (2018) Prolonged co-treatment with HGF sustains epithelial integrity and improves pharmacological rescue of Phe508del-CFTR. *Sci. Rep.* **8,** 13026 CrossRef Medline
43. Goll, D. E., Thompson, V. F., Li, H., Wei, W., and Cong, J. (2003) The calpain system. *Physiol. Rev.* **83,** 731–801 CrossRef Medline
44. Averna, M., Stifanese, R., De Tullio, R., Minicucci, L., Cresta, F., Palena, S., Salamino, F., Pontremoli, S., and Melloni, E. (2011) Evidence for alteration of calpain/calpastatin system in PBMC of cystic fibrosis patients. *Biochim. Biophys. Acta* **1812,** 1649–1657 CrossRef Medline
45. Galietta, L. J., Haggie, P. M., and Verkman, A. (2001) Green fluorescent protein-based halide indicators with improved chloride and iodide affinities. *FEBS Lett.* **499,** 220–224 CrossRef Medline
46. Yang, H., Shelat, A. A., Guy, R. K., Gopinath, V. S., Ma, T., Du, K., Lukacs, G. L., Taddei, A., Folli, C., Pedemonte, N., Galietta, L. J., and Verkman, A. S. (2003) Nanomolar affinity small molecule correctors of defective Delta F508-CFTR chloride channel gating. *J. Biol. Chem.* **278,** 35079–35085 CrossRef Medline
47. Caputo, A., Hinzpeter, A., Caci, E., Pedemonte, N., Arous, N., Di Duca, M., Zegarra-Moran, O., Fanen, P., and Galietta, L. J. (2009) Mutation-specific potency and efficacy of cystic fibrosis transmembrane conductance regulator chloride channel potentiators. *J. Pharmacol. Exp. Ther.* **330,** 783–791 CrossRef Medline
48. Sharma, M., Pampinella, F., Nemes, C., Benharouga, M., So, J., Du, K., Bache, K. G., Papsin, B., Zerangue, N., Stenmark, H., and Lukacs, G. L. (2004) Misfolding diverts CFTR from recycling to degradation: quality control at early endosomes. *J. Cell Biol.* **164,** 923–933 CrossRef Medline
49. Yao, X., Thibodeau, A., and Forte, J. G. (1993) Ezrin-calpain I interactions in gastric parietal cells. *Am. J. Physiol.* **265,** C36–C46 CrossRef Medline
50. Shcherbina, A., Bretscher, A., Kenney, D. M., and Remold-O'Donnell, E. (1999) Moesin, the major ERM protein of lymphocytes and platelets, differs from ezrin in its insensitivity to calpain. *FEBS Lett.* **443,** 31–36 CrossRef Medline
51. Sasaki, T., Kishi, M., Saito, M., Tanaka, T., Higuchi, N., Kominami, E., Katunuma, N., and Murachi, T. (1990) Inhibitory effect of di- and tripeptidyl aldehydes on calpains and cathepsins. *J. Enzym. Inhib.* **3,** 195–201 CrossRef Medline
52. Shenoy, A. M., and Brahmi, Z. (1991) Inhibition of the calpain-mediated proteolysis of protein kinase C enhances lytic activity in human NK cells. *Cell. Immunol.* **138,** 24–34 CrossRef Medline
53. Hutt, D. M., Loguercio, S., Roth, D. M., Su, A. I., and Balch, W. E. (2018) Correcting the F508del-CFTR variant by modulating eukaryotic translation initiation factor 3-mediated translation initiation. *J. Biol. Chem.* **293,** 13477–13495 CrossRef Medline
54. Moyer, B. D., Duhaime, M., Shaw, C., Denton, J., Reynolds, D., Karlson, K. H., Pfeiffer, J., Wang, S., Mickle, J. E., Milewski, M., Cutting, G. R., Guggino, W. B., Li, M., and Stanton, B. A. (2000) The PDZ-interacting domain of cystic fibrosis transmembrane conductance regulator is required for functional expression in the apical plasma membrane. *J. Biol. Chem.* **275,** 27069–27074 Medline
55. Cushing, P. R., Fellows, A., Villone, D., Boisguérin, P., and Madden, D. R. (2008) The relative binding affinities of PDZ partners for CFTR: a biochemical basis for efficient endocytic recycling. *Biochemistry* **47,** 10084–10098 CrossRef Medline
56. Bhattacharya, S., Dai, Z., Li, J., Baxter, S., Callaway, D. J., Cowburn, D., and Bu, Z. (2010) A conformational switch in the scaffolding protein NHERF1 controls autoinhibition and complex formation. *J. Biol. Chem.* **285,** 9981–9994 CrossRef Medline
57. Short, D. B., Trotter, K. W., Reczek, D., Kreda, S. M., Bretscher, A., Boucher, R. C., Stutts, M. J., and Milgram, S. L. (1998) An apical PDZ protein anchors the cystic fibrosis transmembrane conductance regulator to the cytoskeleton. *J. Biol. Chem.* **273,** 19797–19801 CrossRef Medline
58. Reczek, D., and Bretscher, A. (1998) The carboxyl-terminal region of EBP50 binds to a site in the amino-terminal domain of ezrin that is masked in the dormant molecule. *J. Biol. Chem.* **273,** 18452–18458 CrossRef Medline
59. Li, J., Dai, Z., Jana, D., Callaway, D. J., and Bu, Z. (2005) Ezrin controls the macromolecular complexes formed between an adapter protein Na^+/H^+ exchanger regulatory factor and the cystic fibrosis transmembrane conductance regulator. *J. Biol. Chem.* **280,** 37634–37643 CrossRef Medline
60. Abbattiscianni, A. C., Favia, M., Mancini, M. T., Cardone, R. A., Guerra, L., Monterisi, S., Castellani, S., Laselva, O., Di Sole, F., Conese, M., Zaccolo, M., and Casavola, V. (2016) Correctors of mutant CFTR enhance subcortical cAMP-PKA signaling through modulating ezrin phosphorylation and cytoskeleton organization. *J. Cell Sci.* **129,** 1128–1140 CrossRef Medline
61. van Meegen, M. A., Terheggen-Lagro, S. W., Hoelen, H., Braakman, I., Coffer, P. J., van der Ent, C. K., and Beekman, J. M. (2009) Analysis of CFTR expression in immune cell subsets of peripheral blood. *J. Cyst. Fibros* **8,** S56 CrossRef
62. Johansson, J., Vezzalini, M., Verzè, G., Caldrer, S., Bolognin, S., Buffelli, M., Bellisola, G., Tridello, G., Assael, B. M., Melotti, P., and Sorio, C. (2014) Detection of CFTR protein in human leukocytes by flow cytometry. *Cytometry A* **85,** 611–620 CrossRef Medline
63. Antigny, F., Norez, C., Becq, F., and Vandebrouck, C. (2008) Calcium homeostasis is abnormal in cystic fibrosis airway epithelial cells but is normalized after rescue of F508del-CFTR. *Cell Calcium.* **43,** 175–183 CrossRef Medline
64. Antigny, F., Norez, C., Cantereau, A., Becq, F., and Vandebrouck, C. (2008) Abnormal spatial diffusion of Ca^{2+} in F508del-CFTR airway epithelial cells. *Respir. Res.* **9,** 70 CrossRef Medline
65. Norez, C., Antigny, F., Becq, F., and Vandebrouck, C. (2006) Maintaining low Ca^{2+} level in the endoplasmic reticulum restores abnormal endogenous F508del-CFTR trafficking in airway epithelial cells. *Traffic* **7,** 562–573 CrossRef Medline
66. Ribeiro, C. M., Paradiso, A. M., Carew, M. A., Shears, S. B., and Boucher, R. C. (2005) Cystic fibrosis airway epithelial $Ca^{2+}{}_i$ signaling. *J. Biol. Chem.* **280,** 10202–10209 CrossRef Medline
67. Hoskin, V., Szeto, A., Ghaffari, A., Greer, P. A., Côté, G. P., and Elliott, B. E. (2015) Ezrin regulates focal adhesion and invadopodia dynamics by altering calpain activity to promote breast cancer cell invasion. *Mol. Biol. Cell.* **26,** 3464–3479 CrossRef Medline
68. Donkor, I. O. (2011) Calpain inhibitors: a survey of compounds reported in the patent and scientific literature. *Expert Opin. Ther. Pat.* **21,** 601–636 CrossRef Medline
69. Donkor, I. O. (2014) An updated patent review of calpain inhibitors (2012–2014). *Expert Opin. Ther. Pat.* 10.1517/13543776.2014.982534
70. Almaça, J., Dahimène, S., Appel, N., Conrad, C., Kunzelmann, K., Pepperkok, R., and Amaral, M. D. (2011) Functional genomics assays to study CFTR traffic and ENaC function. *Methods Mol. Biol.* **742,** 249–264 CrossRef Medline